Investigating the role of macromolecular crowding in 3D organisation of Escherichia Coli nucleoid

A Thesis

Submitted to

Indian Institute of Science Education and Research Pune
Dr. Homi Bhabha Road,
Pashan, Pune 411008, India

in Partial Fulfilment of the Requirements
for the BS-MS Dual Degree Programme

by

Paritosh Gupta
(Roll No. 20211214)

May 21, 2026

Supervisor: Dr. Vittore Scolari
Co-supervisor: Prof. Marco Cosentino-Lagomarsino

Certificate

This is to certify that this dissertation entitled *Investigating the role of macromolecular crowding in 3D organisation of Escherichia Coli nucleoid* towards the partial fulfilment of the BS-MS dual degree programme at the Indian Institute of Science Education and Research, Pune represents work carried out by **Paritosh Gupta** under the supervision of **Dr. Vittore Scolari** and **Prof. Marco Cosentino-Lagomarsino** during the academic year 2025-2026.

Dr. Vittore Scolari
Supervisor

Committee:
Dr. Vittore Scolari
Prof. Marco Cosentino-Lagomarsino
Prof. Shivprasad Patil

This thesis is dedicated to My mom, Versha, my grandmom Bimlesh, my sisters, Kriti and Shuchi and everyone else who has sacrificed for me to get every opportunity that got me here.

Declaration

I hereby declare that the matter embodied in the report entitled *"Investigating the role of macromolecular crowding in 3D organisation of Escherichia Coli nucleoid "* is the result of work carried out by me at the Institut Curie, Paris, France and Instituto Fondazione di Oncologia Molecolare ETS, Milan, Italy , under the supervision of Dr. Vittore Scolari and Prof. Marco Cosentino-Lagomarsino, and the same has not been submitted elsewhere for any other degree. Wherever others contribute, every effort is made to indicate this clearly, with due reference to the literature and acknowledgement of collaborative research and discussions.

Paritosh Gupta
Roll Number: 20211214

Acknowledgments

I am deeply grateful to Prof. Marco Cosentino lagomarsino (MCL) for putting me in contact with Dr. Vittore Scolari and for making this project possible. I am thankful to Vittore, the supervisor, for being exactly what I needed when I needed. I admire his guidance, patience, kindness and passion for science. I am deeply grateful to him for being there as a mentor to me. I am also grateful to MCL for helping us with the project in Paris and later for hosting me in Milan and granting me the opportunity to explore a new and unique project. I would also like to thank Prof. Laura Finzi, David Dunlap, Narendar Kolimi, Sumitabha Brahmachari, and Jin Qian for sharing their valuable experimental data and for several insightful conversations regarding the project. A special thanks to Dr. Antoine Coulon for providing valuable discussion sessions and feedback and hosting me in the lab. I would also like to thank Francoise Wyart Brochard, Prof. Jean Francois Joany, and Dr. Pierre Sens for their valuable insights and feedback on the project. I would also like to thank Samuele lipani, Dr. Jing Xie, Melanie Miranda, Sarah Sadik, Kyra Borgman, Ilham Ladid, Julia Ronsch and Tony Makadissy for welcoming me in the Coulon Lab, and making me feel comfortable. And a special thanks to Samuele, Melanie, Jing, Asya, Abhrotanu, Shubhamay, Pablo, Roccio and Yara for some scientific discussions, friendly banter and a lot of happy memories in Paris.

I want to thank Vittore, the friend, for taking me in his home and Liza for putting up with me for 6 entire months. I am grateful to you for the conversations, the food, the sleep experiments, and for being my family when I had none.

I want to thank two of my most valuable friends, Chinmayee and Authisha, for seeing me through some of my toughest times, not only during this thesis, but also during my time at IISER Pune. And finally, to all my friends in IISER Pune, a special thanks to you all for making these years the best I have ever had.

A special mention to Institut Curie and IFOM-ETS for sharing their knowledge, the administration, especially Marie, Marina and Alessia for making my time in Paris and Milan as comfortable as possible and IISER Pune for allowing this thesis to occur. Last but certainly not least, I am eternally indebted to my family for motivating me and making me capable of taking on these challenges.

Contributions

I/We declare that the use of Generative AI in this thesis did not extend beyond what is described in Section 4.6.2 of the 'Guidelines for Generative AI usage at IISER Pune, This work was primarily human-created. AI was used to make stylistic edits, such as changes to structure, wording, and clarity. AI-generated content was reviewed and approved. The following model(s) or application(s) were used: ChatGPT (GPT 5.3) by OpenAI and Microsoft Copilot (AI companion, March 2026).

Contents

Acknowledgments 4

Contributions 5

Contents 6

List of Figures 8

List of Tables 9

Notation 10

Abstract 11

1 Introduction 12

1.1 The Biological problem . . . 12
1.2 Basics of the bacterial nucleoid architecture . . . 12
1.3 The physical problem . . . 15
1.3.1 Nucleoid as a phase separation between cytoplasm and DNA . . . 15
1.3.2 Bacterial DNA as a semi-flexible polymer . . . 16
1.3.3 Polymer collapse and the PSI transition . . . 17
1.4 Experimental and computational evidence . . . 17
1.4.1 Optical Tweezers . . . 17
1.4.2 Magnetic Tweezers . . . 19
1.4.3 Experimental evidence . . . 21
1.4.4 Computational modelling and simulations . . . 21
1.5 Analytical theory to describe macromolecular crowders as a compacting agent . . . 22

2 Worm Like Chain Model 24

2.1 Worm-like chain model . . . 24
2.2 Marko-Siggia model or the Stretching WLC polymer . . . 26
2.3 Depletion interactions as an effective compaction force due to crowders . 28

3 The Partition Function Z **30**

4 Understanding and calculating the impact of the crowders **32**

4.1 excluded volume due to the polymer and the effective free energy 32

4.2 Incorporating the transverse fluctuations in the excluded volume 34

4.2.1 Perturbative expansion of the excluded volume 35

4.2.2 Calculation of $\langle \rho^2 \rangle$ 36

4.3 Deriving the force Extension relation 38

4.3.1 Force-extension relationship in the absence of transverse fluctuations 38

4.3.2 Force extension relationship in presence of transverse fluctuations 38

5 Results **40**

5.1 The Osmotic force has a compacting effect on the polymer in the Zeroth order 40

5.2 The Transverse fluctuations tend to swell the polymer 42

5.3 Asymptotic behaviour of $g(\lambda)$ and the force extension relationship 43

6 Discussion **45**

7 Conclusion **48**

Bibliography **49**

List of Figures

1.1 Supercoiling in *E. coli* 14
1.2 *E coli* under a transmission electron microscope(TEM) 16
1.3 Infographic of force balance in an optical tweezer 18
1.4 Standard elements of an optical-tweezer setup 19
1.5 Infographic for Magnetic tweezer experiments 20
1.6 Standard elements of a magnetic tweezer setup 20
1.7 Coarse-grained model of a polymer-crowder system 21

2.1 Illustration of a standard Worm-like chain 24
2.2 Force-extension for the Marko-Siggia theory 26

4.1 Illustration of a fluctuation polymer 34
4.2 Illustration of the extra excluded volume due to fluctuations 35
4.3 Illustration of excluded trajectories due to fluctuations 36

5.1 Force-extension relationship for the zeroth-order approximation 40
5.2 Compaction force due to the crowders as a function of ϕ 41
5.3 Force-extension relationship for the second-order approximation 42
5.4 Contribution of fluctuation-dependent correction to the force-extension . 43

List of Tables

1 Important notation used across the report 10

Notation

To help the reader navigate through the specific notation in this thesis, we have listed all the necessary symbols and notation in alphabetical order, first Latin, then Greek.

A	bare persistence length of the polymer
c	Concentration of crowders
f	Applied external force
f^*	Collapse force applied by the crowders on the polymer
f_c	Characteristic force
k_B	Boltzmann Factor
L	Contour length of the polymer
r	Radius of the monodisperse crowders
r_0	Radius of the DNA monomer
s	Arc length coordinate of the polymer
T	Temperature
z	molecule extension
β	Inverse temperature $\beta = \frac{1}{k_B T}$
$\hat{z}$	Pulling direction
ϕ	Volume fraction
ρ	Fluctuation radius of the DNA
$\tilde{f}$	Effective force on the polymer
$\hat{\mathbf{t}}(s)$	Tangent vector over the arc length coordinate
$\mathbf{t}_\perp(s)$	Orthogonal component of the tangent vector
$\mathbf{u}_\perp(s)$	Orthogonal displacement of the chain
ξ	Force dependent correlation length

Table 1

Abstract

In this report, we present a theory to understand the effects of osmotic pressure due to neutral macromolecular crowders on double-stranded DNA or any semiflexible polymer under tension. The leading order effect is a crowder-induced compaction, which acts against the external applied force. This compacting force f^* is dependent upon crowder size r and volume fraction ϕ, high ϕ and small r result in a higher compaction force f^*. At first order in perturbation theory, we calculate a fluctuation-dependent correction to the depletion volume, which competes with the compaction of the polymer for large crowders leading to expansion of the polymer.

1 Introduction

1.1 The Biological problem

The Bacterium *Escherichia coli* is often considered one of the simplest living organisms. It lacks a membrane-bound nucleus and many other compartmentalised structures characteristic of eukaryotic cells [1, 2]. Yet despite its apparent simplicity, *E. coli* poses several significant scientific questions. Among the most striking is the organisation of its genetic material. With a genomic length of $\approx 1.5mm$ and a cellular volume of $\approx 1\mu m^3$, and the nucleoid only occupies roughly $0.2\mu m^3$ [3] of the cellular volume, Simple scaling estimates put the radius of gyration $(R_g) \approx \sqrt{LA}$ suggesting that radius of gyration for the *E coli* nucleoid in free space should be around $\approx 10\mu m$ far exceeding the cellular dimensions. Thus, the bacterial chromosome must be compacted by several orders of magnitude to fit inside the cell while remaining dynamically accessible to the cell's replication and transcription machinery.

1.2 Basics of the bacterial nucleoid architecture

The bacterial chromosome lacks a membrane-bound nucleus and histone-based chromatin organization. Yet, the bacterial nucleoid is not a random blob of DNA; several experiments have revealed that the *E. coli* nucleoid demonstrates a high level of 3-dimensional organization instead of existing like a random polymer coil. The *E. coli* genome is partitioned into hierarchical structures which maintain both DNA accessibility and global chromosome compaction.

Several experimental studies have shown that the nucleoid is organized into domains stabilized by protein binding, DNA topology, and spatial constraints of the cell[1]. Understanding these structural levels is necessary for connecting the physical properties of DNA with the functional organization of the genome.

The chromosome is confined inside the cell with a large number of macromolecules fundamental for cellular function. Many of these macromolecules, such as transcription factors, DNA and RNA polymerases, nucleosomes, and specific enzymes, associate with the DNA, giving rise to nucleoprotein complexes in the bacterial nucleoid. However,

many other macromolecules near the genome do not interact directly but share the same space inside the cell, and interact with the genome via steric interactions.

At the largest scale, the *E coli* chromosome is divided into megabase-sized macrodomains and smaller topological domains. Experiments revealed that distinct chromosomal loci occupied preferential spatial locations in the cell, suggesting a non-random reproducible spatial organization of the genome[4]. Subsequent studies identified macrodomains like Ori, Ter, Left, and Right[4]. Within these macrodomains, the chromosome gets further organized into topological domains, these domains are usually tens of kilobases and contain independent subunits of DNA supercoils, restricting propagation of torsional stress along the chromosome[5].

Beyond this macrodomain organisation, nucleoid-associated proteins (NAPs) also drive organisation. These proteins bind along the chromosome and modulate its conformations through bending, bridging and wrapping of DNA segments. But these NAP-induced structures are unlike histones as they are not specific repeats and act as dynamic modulators of DNA topology[6].

Many NAPs have been identified in *E coli*, like HU, Fis, IHF and H-NS. Each protein varies in its activity but contributes to the compaction of the genome. HU and IHF are known to introduce sharp bends in DNA, facilitating loop formation and local compaction. H-NS is a bridging protein and brings distant sections of DNA closer together, giving rise to higher-order nucleoprotein complexes that contribute to transcriptional silencing and condensation of chromatin [7].

Although there is ample evidence for these NAPs being used for DNA compaction and organization, the NAP-mediated bridging and looping are not enough to explain the overall nucleoid compaction on its own. Instead, experimental evidence suggests that NAPs operate cooperatively with other physical mechanisms like crowding and supercoiling, to achieve the observed compaction in the DNA [8].

Supercoiling is a central component of nucleoid organization. The bacterial chromosome typically sits in a closed topological domain; important processes, such as transcription and replication open up parts of the DNA to get access, in turn increasing torsional stress in the DNA. This stress leads to the formation of supercoiled structures in which the DNA double helix becomes over- or underwound relative to the relaxed state[9].

The DNA in the nucleoid sits in a slightly underwound state compared to its relaxed state. This results in negative supercoiling, promoting the formation of plectonomic structures, which causes the DNA to wrap around itself, forming intertwined loops. These plectonomes also provide an effective compaction while reducing stress on the polymer during cellular processes.

In eukaryotes, the DNA uses well-categorized structural mechanisms to achieve the required compaction. The genome first wraps around histone octamers, which further fold into higher-order chromatin structures within a membrane-bound nucleus[6]. This strat-

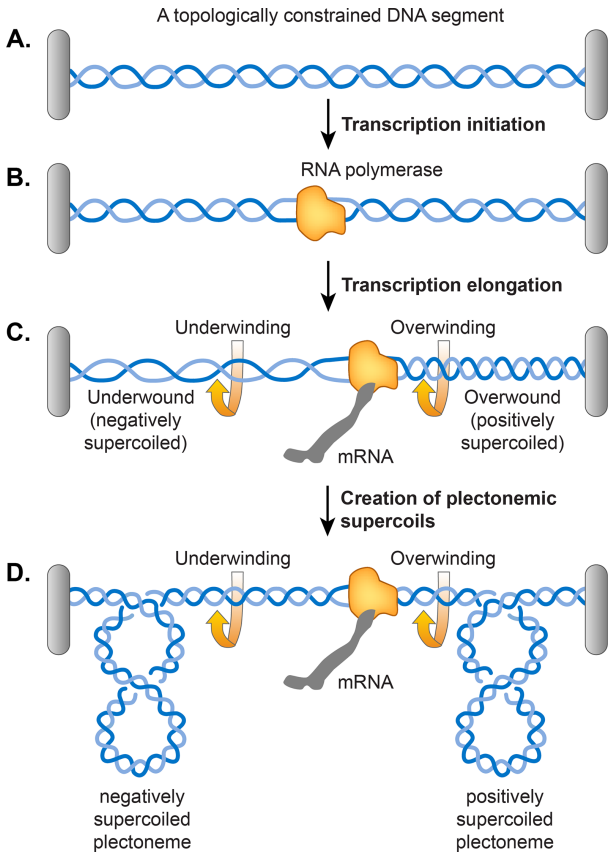

Figure 1.1: The figure shows a topologically constrained DNA segment undergoing supercoiling due to the action of macromolecular machinery of the organism. (A) shows a topologically constrained DNA segment where the constraint could be a protein or membrane anchor. (B) shows the accommodation of RNA polymerase for transcription initiation of this segment of DNA. (C) shows an elongation of the DNA due to the removal of the helical turns by the RNA polymerase, as the RNA polymerase itself cannot rotate around the helical axis of the DNA. This elongation due to the opening of helical turns of DNA causes overwinding and underwinding of the DNA, leading to the formation of plectonemes with positive supercoiling in the overwound region and negative supercoils in the underwound region. The figure has been borrowed from [2]

egy requires specific protein-DNA interactions and machinery to regulate accessibility and maintain organization. But as is known, *E. coli* lacks any such machinery or a bounded membrane for its nucleoid. Although the bacterial chromosome uses nucleoid-associated proteins (NAPs) to introduce bending, bridging and supercoiling[6, 9, 10], these interactions alone prove to be insufficient. Instead, the chromosome organization in bacteria appears to have a cooperative dependence on these NAPs and passive, generic physical forces such as confinement and molecular crowding[8]. Indeed, macromolecules tend to occupy upwards of 40% of bacterial volume. This contrast raises the question: to what extent are these passive mechanisms responsible for the large-scale DNA compaction and organization in prokaryotic cells?

1.3 The physical problem

Now that we have an understanding of the biological context of the DNA compaction problem. It is of interest to understand the progress that has been made to solve this as a question based on physics.

1.3.1 Nucleoid as a phase separation between cytoplasm and DNA

Beyond compaction at the level of individual polymer conformations, fluorescence microscopy revealed that the bacterial nucleoid is "phase separated" from the surrounding cytoplasm, and the chromosome occupies a distinct protein-sparse region near the center of the cell. While the segregation is not exactly an equilibrium phase transition in the thermodynamic sense, it is interpreted as an entropy-driven demixing driven by excluded-volume interactions and osmotic pressure. The DNA-rich region tends to exclude macromolecules(proteins) to the exterior, exerting an outward stress on the cell membrane, which is also linked with cellular growth [11]. The crowder phase (characterized by the high diffusive mobility and osmotic pressure of the free molecules in the system), in turn, exerts a reciprocal osmotic force on the DNA polymer network, compacting the DNA and causing it to phase separate [12, 13]. The physical principle behind this crowder-driven compaction and separation is entropic and related to the depletion interactions first described by Asakura and Oosawa in 1954 [14]. In this framework, small particles are excluded from a region surrounding large particles. When the excluded volumes of two large particles overlap, the volume available to the smaller particles increases, which maximizes entropy, and this gain in entropy physically manifests as an effective attraction between the large bodies.

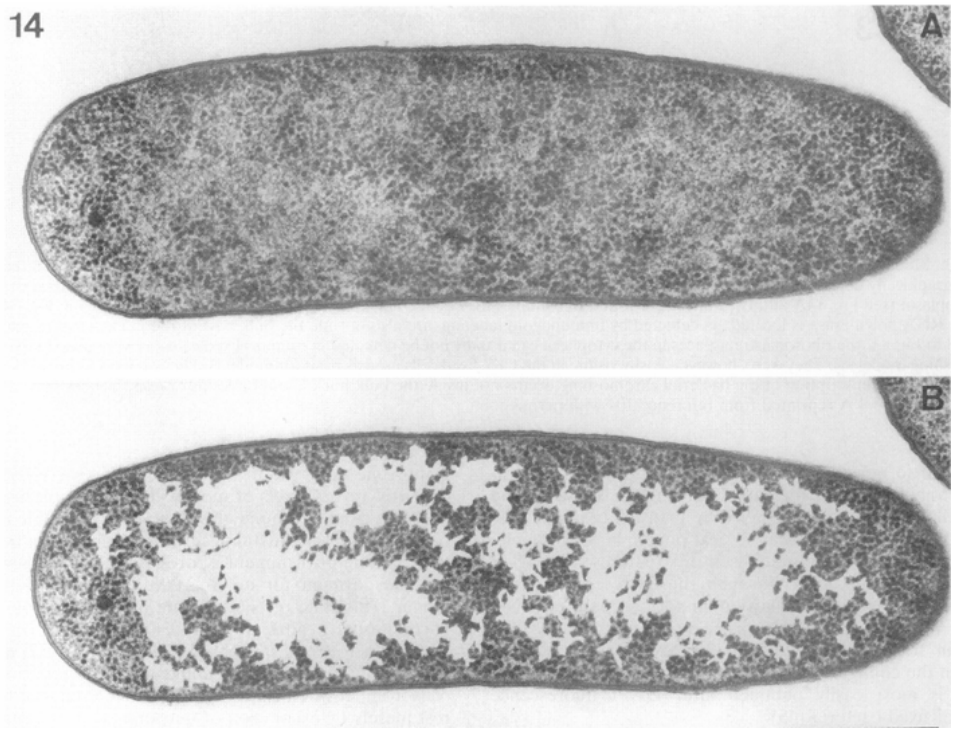

Figure 1.2: An image of the nucleoid following Cryofixation followed by Freeze-stabilization (CFS) showing thin sections of growing E.coli. These images show regions of the nucleoid that are depleted of ribosomes. Panels A and B show the same section; in panel B, the ribosome-free spaces are enhanced by colouring by hand. The image has been taken from [15]

1.3.2 Bacterial DNA as a semi-flexible polymer

To understand how these biological and physical mechanisms work together to achieve the high degree of compaction while maintaining accessibility for cellular processes, it is useful to study the physical properties of the DNA itself. To that end, the DNA is investigated from the perspective of polymer physics.

From a physical perspective, DNA is a semi-flexible polymer characterized by its bare persistence length (A) of approximately $50nm$ under physiological conditions. The contour length (L) of DNA in bacteria far exceeds its persistence length, placing the question firmly in the domain of long-chain polymers. Thus, we are inclined to look at the statistics of semi-flexible polymers under confinement and in crowded environments

In the context of bacterial DNA, the chromosome can be viewed as a large extended object immersed in a bath of smaller crowders. Overlap of excluded volumes between different segments of the polymer increases the entropy of the crowders and thus generates an effective self-attraction of the DNA. Because there is no interaction between DNA and crowders, this DNA compaction is purely physical.

1.3.3 Polymer collapse and the PSI transition

The collapse of a polymer from a swollen coil to a compact globule has been studied in polymer physics[16, 17]. In a good solvent, polymer solvent interactions dominate, and the polymer takes an extended conformation. In a poor solvent, the effective monomer-monomer attraction leads to the polymer's collapse into a dense globule. The transition between these regimes occurs at the θ temperature. Foundational theoretical models of this phenomenon were developed by Paul J. Flory[18] and were later refined through scaling concepts by Pierre-Gilles de Gennes[19]. But the compaction of polymers induced by polymers and salt in vitro is fundamentally different from the θ transition and is referred to as the ψ transition for the Polymer-and-Salt induced (PSI) transition. Early experiments with neutral polymers like polyethlene glycol (PEG) in a high concentration of salt showed evidence of compaction in DNA[20]. The ψ transition is not driven by the temperature-dependent solvent quality; it is dependent upon the excluded-volume effects and osmotic pressure from external macromolecules. This key difference between θ and ψ transition must be highlighted as it makes the latter susceptible to changes in the crowder concentration and size.

1.4 Experimental and computational evidence

Before diving into the experimental evidence itself, it is useful to understand the key experimental techniques that have enabled these discoveries.

One of the key techniques for inferring polymer and DNA behaviour is to characterize the molecule's response under tension *in vitro* using force spectroscopy. Tweezers(optical and magnetic) are a key experimental technique to study the polymer response under tension.

1.4.1 Optical Tweezers

Optical traps are one of the most versatile tools for single-molecule manipulation. The technique relies on a focused laser, creating a 3D potential well trapping dielectric particles like micron-sized beads. The bead experiences a potential gradient, thus a restoring force directed towards the centre of the trap due to an induced dipole interaction with the optical field gradient.

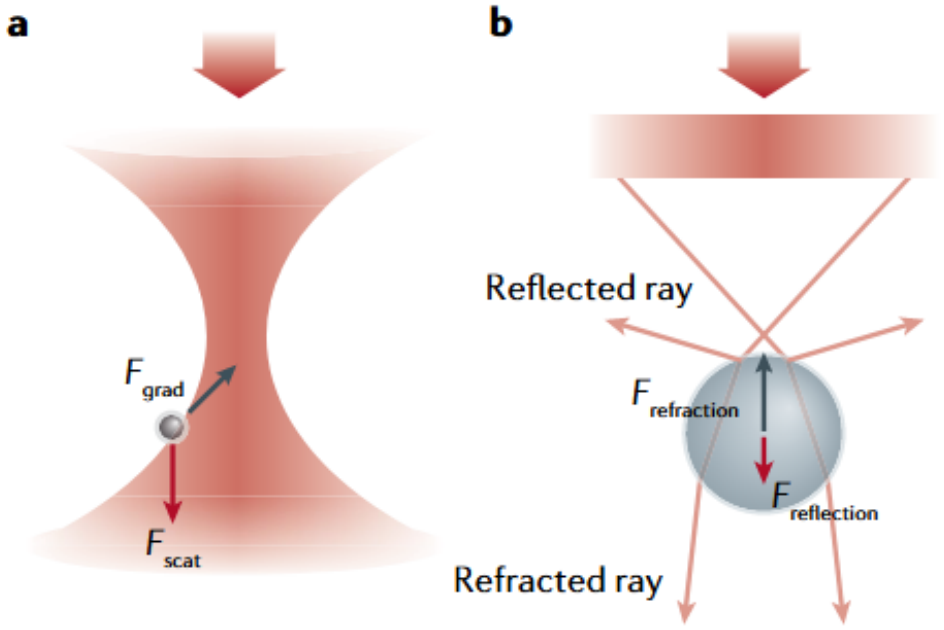

Figure 1.3: The image shows the forces acting on a dielectric sphere interacting with a light gradient, with the incident beam focused by a high numerical aperture lens. In panel (a), the particle(smaller than the light wavelength) is being pushed away from the centre, along the direction of light propagation, by the scattering force($F_{scat}, redarrow$), and the particle experiences a restoring gradient force (F_{grad}) bringing it towards the centre of the beam. In panel (b), the dielectric particle shown is bigger than the wavelength of the light beam. This leads to reflection or refraction of light(pink arrows). This leads to a change in direction, correspondingly a change in momentum, which in turn results in an equal but opposite change in momentum of the dielectric bead. The reflected rays lose forward momentum, resulting in a pushing force ($F_{reflection}$) pushing the bead along the direction of propagation, and refraction leads to rays that are deflected forward due to their high incidence, generating a reactive force ($F_{refraction}$) pulling the bead towards the focus. The images are borrowed from [21]

Typically, a biomolecule will be tethered between two micron-sized beads, one held in the optical trap and the other attached to a micropipette or surface. By displacing the bead in the trap relative to the trap centre. For small displacements, the trap acts like a Hookean spring, allowing force to be calculated from the displacement of the bead. Optical tweezers can apply forces ranging from 0.1 to 100 piconewtons while maintaining a sub-nanometer precision and sub-millisecond time resolution, allowing optical tweezers to be used with the manipulation of DNA, RNA as well as active molecular motors.

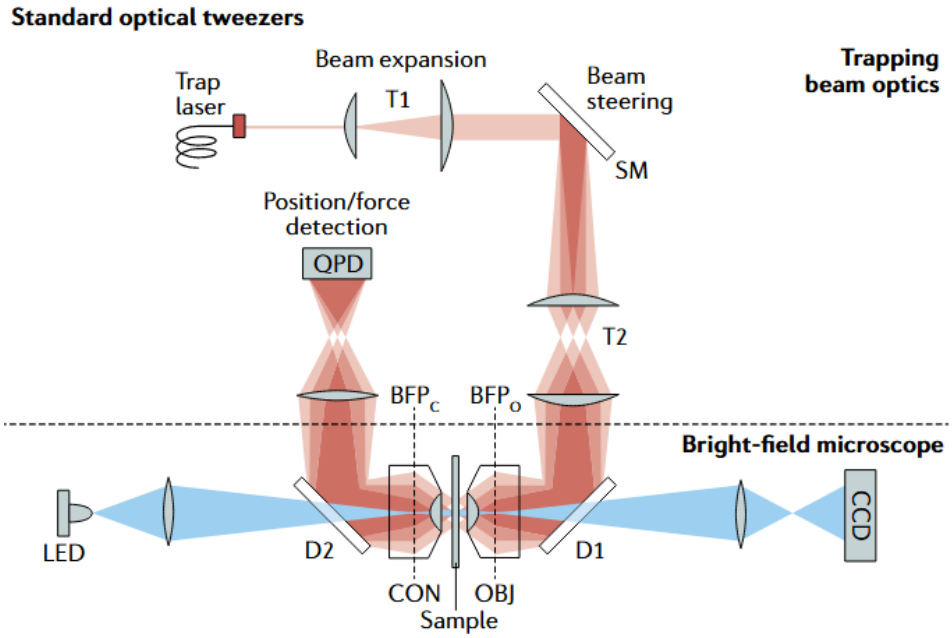

Figure 1.4: The figure depicts the optical layout of a standard single-beam optical trap. A standard set would contain a high-powered optical laser that generates the trapping beam. The beam will pass through a telescope, which expands it. There will be some beam-steering machinery controlling the beam axis. A high numerical aperture objective(OBJ) that focuses the beam on the sample. The image is borrowed from [21]

1.4.2 Magnetic Tweezers

Magnetic tweezers use a robust technique to manipulate single molecules using magnetic forces. The apparatus is typically made of a pair of permanent magnets positioned above a microscope chamber containing super-magnetic beads attached to the molecule under consideration. The Magnetic field gradient generated by the magnets exerts a force on the bead, pulling it along the gradient and thereby stretching the molecule attached.

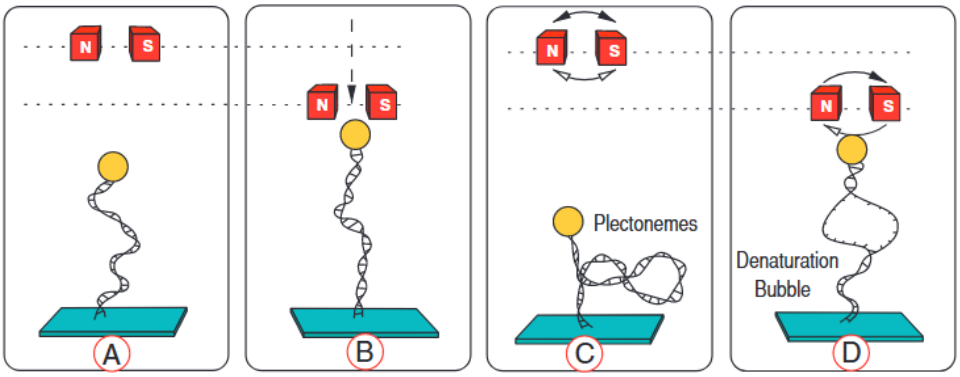

Figure 1.5: The image depicts the most common types of experiments conducted using magnetic tweezers. Where N and S represent the north and south poles of the permanent magnets. Panels A and B illustrate the pulling experiments, where the magnetic bead gets pulled under the influence of the magnetic field. These experiments are essential in determining the force extension behaviour of polymers. Panels C and D are representative of the twisting application of magnetic tweezers, where a torque can be applied by rotating the magnets. These experiments are useful in studying the supercoiling behaviour of DNA under torsional stress.

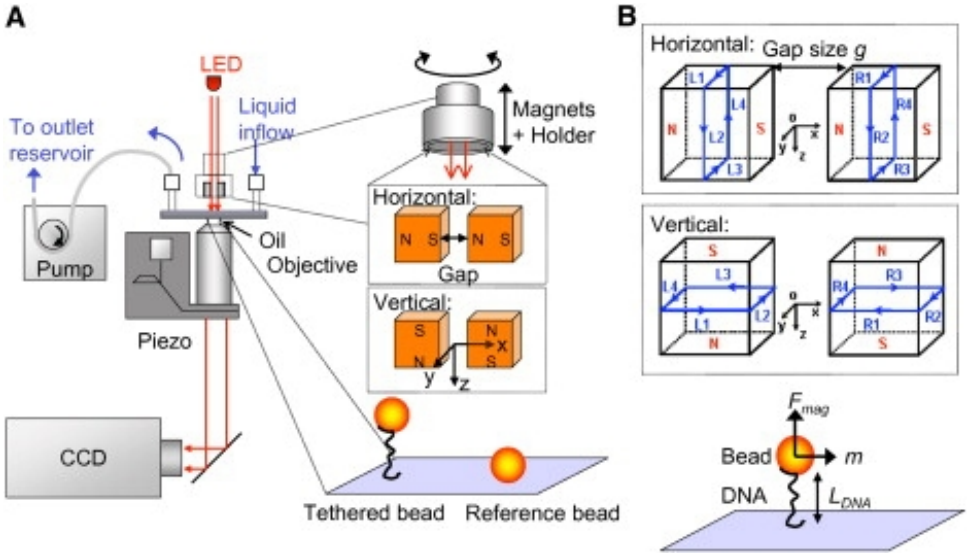

Figure 1.6: The figure depicts the standard elements of a magnetic tweezer setup. (A) A schematic of major components of the magnetic tweezer, including the magnets, holder, objective, cameras, tethered sample and piezo actuators. (B)A schematic for the flow of current and magnetic fields to conduct vertical and horizontal pulling experiments using magnetic tweezers.

Magnetic tweezers use a robust technique to manipulate single molecules using magnetic forces. The apparatus is typically made of a pair of permanent magnets positioned above a microscope chamber containing super-magnetic beads attached to the molecule under consideration. The Magnetic field gradient generated by the magnets exerts a force on the bead, pulling it along the gradient and thereby stretching the molecule attached.

One end of the molecule will be attached to a glass surface, while the other end is attached to the bead. Since the gradient varies slowly with position, the tweezers provide a nearly constant environment. Magnetic tweezers can also be used to apply torque to the molecule, facilitating studying the topology, including supercoiling for DNA and for studying the activity of enzymes such as topoisomerases.

1.4.3 Experimental evidence

Experimental studies also provide strong evidence for the compaction of DNA through macromolecular crowding. Osmotic shock-driven condensation is observed in the *E coli*, resulting in a reduction in the nucleoid volume following an increase in the salt concentration [22]. The osmotic shock drives out the water from inside the cell, thereby increasing the macromolecular concentration inside the cell. The nucleoid was observed to show a more significant reduction in volume compared to the cytoplasmic volume, suggesting a cooperative compaction mechanism consistent with crowding-induced collapse[23]. Similar effects were also observed with eukaryotic chromatin in human cell lines: an increase in density of molecular crowders has been correlated to chromosomal mitotic condensation post the dissolution of the nuclear envelope.[24]

Complimentary *in vitro* experiments using purified DNA and neutral crowders such as PEG have also shown direct compaction with an increase in crowder concentration [8, 25, 26]. Experiments performed on Intrinsically Disordered Proteins(IDPs) using Single-molecule Forster resonance energy transfer(SM-FRET) demonstrate compaction of the polymer under increasing crowder concentrations and increasing crowder sizes[27]. Suggesting relevance of the parameters, ϕ and crowder size r. Through these experiments, one can systematically tune the system by changing the volume fraction and crowder size. Together *in vivo* and *in vitro* observations support the idea that crowding at physiological densities can regulate chromosome organization.

1.4.4 Computational modelling and simulations

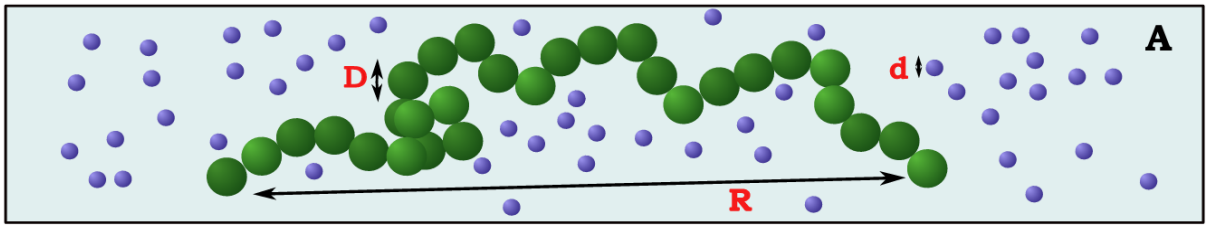

Figure 1.7: The figure is a depiction of bead spring polymer in a bath of spherical crowders of diameter d. The figure highlights all the key parameters relevant to molecular dynamics simulation-based studies. The figure is borrowed from [28]

Experimental results and theory have also been complemented by molecular dynamics simulations reproducing crowder-mediated compaction of polymer models *in silico* [22, 28–31]. A typical MD simulation would consist of L spherical beads of radius D connected by springs of similar extension immersed in a bath of smaller spheres or crowders of radius d with density c. These simulations were able to identify that the volume fraction of the crowder $\phi = \frac{4\pi d^3 c}{3}$ and the relative size of the crowder $\frac{D}{d}$ are the key parameters in determining the strength of crowder-induced polymer compaction.

While simulations were able to show and quantify the crowders' ability to exert force and compact the polymer, there are limits to this approach as well. For starters, as with all empirical derivations, simulation approaches are only valid for the range of investigated parameters, and one cannot simply extrapolate these results to a wider range of parameters with brevity. Furthermore, it is a challenge to improve this type of simulation, as a reduction of d/D by a factor of x with a constant volume fraction ϕ entails an increase in the number of simulated particles of $O(x^3)$. Similarly, an increase in the polymer length by a factor x entails, due to the scaling of polymer dynamics, an increase in the simulated volume and number of particles by $O(x^{5/2})$. More fundamentally, the bead spring model is not a good polymer to simulate DNA due to its significantly slender nature (bending stiffness).

1.5 Analytical theory to describe macromolecular crowders as a compacting agent

Despite extensive work on crowding-induced collapse, far less attention has been devoted to the modification of a polymer's mechanical response under crowding conditions. In particular, it remains unclear how bending fluctuations and depletion-induced osmotic forces come together to tune the polymer's mechanical response. While experiments and simulations demonstrate compaction, it is of interest to analytically illuminate the link between microscopic steric interactions and macroscopic mechanics of the polymer. The objective of this thesis is to construct a theoretical description of crowding-induced forces acting on a semiflexible polymer. with particular emphasis on bacterial DNA. We aim to bridge the gap between classical polymer physics, depletion interaction theory and single-molecule elasticity.

The structure of the thesis is as following First, we review the statistical mechanics of semiflexible polymers, the worm-like chain model and the Marko-Siggia model, then we will introduce the depletion interactions and osmotic pressure in crowded media following which we will derive an effective free energy for the stretched polymer in a bath of crowders and use the Gibbs ensemble framework to derive analytical results for the modified force-extension relation. The results will be presented and discussed within the context

of double-stranded DNA. Finally, we will evaluate the implications of our findings for chromosome organisation in the larger picture.

By developing an analytical approach to crowding-induced compaction, this work aims to extend the conceptual clarity and predictive power beyond the existing simulation-based studies.

2 Worm Like Chain Model

This chapter describes the theoretical background necessary for our work, the Worm-like chain (WLC) model, the Marko-Siggia model[32], which adapts the WLC model to external stretching, and the concept of depletion interactions that appear due to the entropic effects of the crowders.

2.1 Worm-like chain model

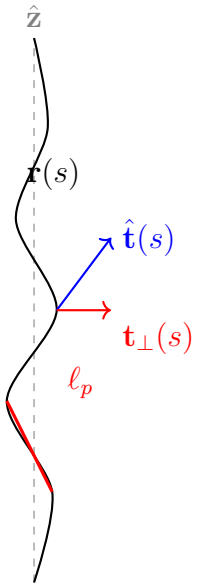

Figure 2.1: Illustration of a Worm-like chain. The red segment indicates one persistence length ℓ_p measured along the polymer contour. The unit tangent vector $\hat{\mathbf{t}}(s)$ and its transverse component $\mathbf{t}_\perp(s)$ are shown at arclength position s. The illustration was created via a TikZ code with assistance from Microsoft Copilot (AI companion, March 2026).

The Worm-like chain (WLC) model, or the Kratky-Porod Model, is a model in polymer physics used to describe semi-flexible polymers. It is a standard model and can be found in any textbook. The following introduction is borrowed from Michael Rubinstein [16]. These polymers are fairly stiff with successive segments pointing in roughly the same direction and with some persistence length.

The WLC model describes a continuously flexible isotropic rod. This is in contrast with the Freely-jointed chain(FJC) polymer, which is only flexible between discrete hinges.

For a polymer of contour length (L), parameterised by $s \in (0, L)$. $\hat{\mathbf{t}}(s)$ is the unit tangent vector to the chain at the point s, and $\mathbf{r}(s)$ is the position vector along the chain as shown in the image. Then:

$$\hat{\mathbf{t}}(\mathbf{s}) = \frac{\partial \mathbf{r}(s)}{\partial s} \tag{2.1}$$

and the end-to-end distance

$$\mathbf{R} = \int_0^L \hat{\mathbf{t}}(s) ds \tag{2.2}$$

The energy associated with the bending of the polymer can be written as

$$E = \frac{k_B T}{2} \int_0^L A \cdot \left(\frac{\partial^2 \mathbf{r}(s)}{\partial s^2} \right)^2 ds \tag{2.3}$$

where A is the persistence length or the characteristic length over which a bend can be made with energy cost $k_B T$, k_B is the Boltzmann constant and T is the absolute temperature. At finite temperatures, the end-to-end distance of the polymer is significantly shorter than the contour length due to thermal fluctuations, resulting in a coiled, random configuration of the undisturbed polymer.

An important quantity of the WLC model is the polymer's orientation correlation function that follows an exponential decay.

$$\langle \hat{\mathbf{t}}(\mathbf{s_1}) \cdot \hat{\mathbf{t}}(\mathbf{s_2}) \rangle = e^{-\frac{|s_1 - s_2|}{A}} \tag{2.4}$$

Another important quantity is the mean-squared end-to-end distance of the polymer ends

$$\langle R^2 \rangle = \langle \mathbf{R} \cdot \mathbf{R} \rangle = 2AL \left(1 - \frac{A}{L} \left(1 - e^{\frac{L}{A}} \right) \right) \tag{2.5}$$

In the long chain limit, i.e. $L >> A$, $\langle R^2 \rangle \to 2AL$, implying that the Kuhn segment is twice the length of the persistent segment.

2.2 Marko-Siggia model or the Stretching WLC polymer

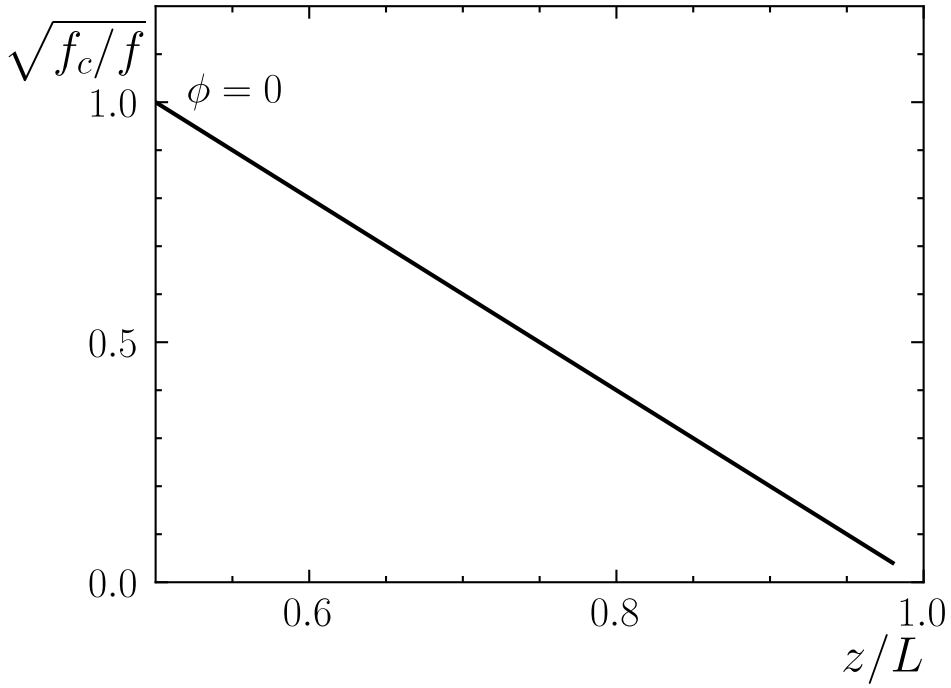

Figure 2.2: The figure represents the force-extension relationship for a worm-like chain under stretching force as per the Marko-Siggia theory. The axes are in the normalized units.

Upon application of force, the polymer begins to stretch, approaching the contour length. For forces less than the characteristic force $f_c = k_B T/A$, the polymer acts like any other freely jointed polymer; the force-extension relationship is linear, and the polymer is organised into *Pincus blobs*. The size of each blob is set by the quantity $k_B T/f$. These blobs are purely entropic in nature.

Upon stretching, as the force on the polymer increases, the blobs first reduce in size and finally, as we approach the characteristic force f_c, the WLC approaches the contour length L, and the tangent vector fluctuates only slightly around $\hat{\mathbf{z}}$. The following calculations in this section are based on the work of John F. Marko and Eric D. Siggia's work [32].

The effective energy of a stretched WLC becomes

$$\frac{E}{k_B T} = \int_0^L \frac{A}{2} \left(\frac{\partial^2 \mathbf{r}(s)}{\partial s^2} \right)^2 ds - fz \tag{2.6}$$

Since the orthogonal fluctuations are small in the strong stretching regime, imposing the condition $|\hat{\mathbf{t}}| = 1$ and the orthogonal components t_x and t_y are considered to be independent, then t_z can be written as a quadratic function of the two-vector $\mathbf{t}_\perp$

$$\mathbf{t}_\perp = [t_x, t_y] \tag{2.7}$$

$$t_z = 1 - {\mathbf{t}_\perp}^2/2 + O({t_\perp}^4) \tag{2.8}$$

to quadratic order $(\partial_s^2 \mathbf{r}(s))^2 = (\partial_s^2 \mathbf{t}_\perp(s))^2$, the the effective energy becomes,

$$\frac{E}{k_B T} = \frac{1}{2}\int_0^L ds \left[A(\partial_s {\mathbf{t}_\perp}^2 + f{\mathbf{t}_\perp}^2\right] - fL \tag{2.9}$$

taking a fourier transform $\tilde{\mathbf{t}_\perp} = \int ds e^{iqs}\mathbf{t}_\perp$ decouples the energy into normal modes

$$\frac{E}{k_B T} = \frac{1}{2}\int_0^L \frac{dq}{2\pi}\left[Aq^2 + f\right]|\tilde{\mathbf{t}_\perp}|^2 - fL \tag{2.10}$$

The average of $t_\perp^2$ at any point s is simply given by the equipartition theorem

$$\langle {\mathbf{t}_\perp}^2\rangle = \int \frac{dq}{2\pi}\langle|\tilde{\mathbf{t}_\perp^2}(\mathbf{q})|\rangle = 2\int \frac{dq}{2\pi}\frac{1}{Aq^2+f} = \frac{1}{(fA)^{1/2}} \tag{2.11}$$

The leading factor in above equation comes from counting both components of $\mathbf{t}_\perp$. The extension, as represented by the black line in the Fig. 2.2 is given by:

$$\frac{\langle z\rangle}{L} = \hat{\mathbf{t}}\cdot\hat{\mathbf{z}} = 1 - \frac{1}{(4fA)^{1/2}} \tag{2.12}$$

The side-to-side excursions of the chain over arc length s, can also be calculated exactly in the gaussian limit using $\mathbf{t}_\perp = \partial_s \mathbf{r}_\perp$

$$R_\perp^2 = \langle[\mathbf{r}_\perp(\mathbf{s}) - \mathbf{r}_\perp(\mathbf{0})]^2\rangle \tag{2.13}$$

$$R_\perp^2 = \frac{2}{f}\left(s - \frac{1 - e^{-s(f/A)1/2}}{(f/A)^{1/2}}\right) \tag{2.14}$$

This model introduces the notion of effective persistence length $\xi = (k_B T A/f)^{1/2}$. For small forces $f \approx (k_b T/A)$, $\xi \approx A$ as one would expect. For even smaller forces, the Gaussian fluctuation approximation for $\mathbf{t}_\perp$ is not applicable anymore. The above equation works for forces down to $f \approx k_b T/A$

2.3 Depletion interactions as an effective compaction force due to crowders

The second virial coefficient is also referred to as the 'excluded volume' parameter because of its interpretation in the case of the hard-core repulsion. The excluded volume is defined as minus the integral of the Mayer function over the whole space [16].

$$v = -\int f(r)\, d^3r = \int (1 - \exp(-U(r)/k_B T))\; d^3r \tag{2.15}$$

The term $U(r)$ contains information about the interaction between two monomers. If typical monomers 'like' each other more than they 'like' the solvent, then $U(r)$ contains an attractive well corresponding to this energy difference. If the monomers are chemically identical to the solvent and there is no energy difference between their interactions, then $U(r)$ will only contain the hard-core repulsion. And, if the monomers like the solvent more than they like each other, then there will be no attractive well in $U(r)$ but an extra repulsion.

For this work, we only consider the effective attractive interaction due to the crowders. The crowders only contain a hardcore repulsion with each other and the monomers. To understand the effective attraction due to crowders, we need to understand the term 'depletion interactions'.

Aasakura and Oosawa first proposed that an attractive force acts between two neutral plates in a bath of colloids [14]. We can generalise this force to other geometries. Monomers in a box of volume V with crowders of volume v. And, consider a shell of thickness equal to the radius of the crowders around the monomer. We call this shell the "particle excluded volume". Due to hard-core repulsion, the crowder cannot enter this volume and the total volume accessible to the crowder becomes $V - Nv$ where N is the number of crowders in the box.

When two monomers come close together, their excluded volumes overlap, thus increasing the volume available to the crowders. This is a higher entropy conformation, thus more favourable. This leads to an effective attraction between the monomers.

Another way to understand this idea is via the osmotic pressure exerted by the crowders on the monomer. If the crowders are homogenously distributed around the monomers, at equilibrium, all forces are balanced. If, due to thermal fluctuation, two monomers come close together such that there are no monomers between them, the pressure contribution from their excluded region vanishes, and a net pressure force will try to bring them together. The potential between the two spheres will be the osmotic pressure Π multiplied by the integrated overlap volume $V_{overlap}$ between two monomers.

Some approximations as we go forward with this work

- Mean Field Approximation: the monomer density is uniform in all space occupied by the polymer.
- Only the entropic forces from the crowders are incorporated in the theory
- The crowder gas is ideal

With this background, we can now proceed to incorporate the effects of the crowders in the Marko-Siggia WLC theory.

3 The Partition Function Z

To write the effective energy of the system, we can write a Hamiltonian that considers the configuration of crowders in space. We need to supplement the general worm-like chain Hamiltonian with a term that considers an interaction between each crowder at position $\mathbf{x}_i$ and the crowder chain. We consider that individual crowders are indexed by i spanning from 1 to N; the concentration of the crowders is $c = N/V$, where V is the experimental volume.

In that case the total energy of the system becomes,

$$\beta E\left[\hat{\mathbf{t}}(s), \{\mathbf{x}_i\}\right] = \beta E_{ch} + \beta E_{cro} \tag{3.1}$$

where

$$\beta E_{ch}\left[\hat{\mathbf{t}}(s)\right] = \int_0^L \mathrm{d}s \left[\frac{A}{2}\left(\partial_s \hat{\mathbf{t}}\right)^2 - \beta f \hat{\mathbf{z}} \cdot \hat{\mathbf{t}}\right], \tag{3.2}$$

and

$$\beta E_{cro}\left[\hat{\mathbf{t}}(s), \{\mathbf{x}_i\}\right] = \int_0^L \mathrm{d}s \left[\sum_i^N U\left(\mathbf{x}_i - \mathbf{u}\right)\right], \quad \text{with} \quad \frac{\partial \mathbf{u}(s)}{\partial s} = \hat{\mathbf{t}}; \tag{3.3}$$

We have assumed low crowder density as we ignore the two-body interaction between crowders, and any higher-order interactions. We also assume overdamped conditions, meaning the inertial mass of the crowders and the chain are both negligible. Given monodisperse crowders of radius r, we set the steric potential as:

$$U(\mathbf{x}) = \begin{cases} \infty & \text{if } |\mathbf{x}| < r \\ 0 & \text{otherwise.} \end{cases} \tag{3.4}$$

The partition function corresponding to the Hamiltonian defined above can be written using the Gibbs distribution, which is path integral over all the conformations of the WLC, integrated over all positions of the crowders over the experimental volume V:

$$Z(f, \beta, N, r, L) = \int \mathcal{D}\left[\hat{\mathbf{t}}(s)\right] \prod_i \int_{V \times N} \mathrm{d}\mathbf{x}_i \exp\left[-\beta E\right]. \tag{3.5}$$

On integrating the partition function over the crowder degrees of freedom, we essentially determine the volume available in the configuration space post-reduction due to

the interaction between the crowders and the polymer, i.e. the strength of the depletion interaction. Given the shape of the potential in Eq.(3.4), the problem reduces to calculating the reduction in the volume accessible to the crowders, δV.

$$\frac{Z'\left[\hat{\mathbf{t}}(s)\right]}{Z_{cro}(N)} = \exp\left[N\log\left(1-\frac{\delta V}{V}\right)\right] \approx \exp\left[-\frac{N\,\delta V}{V}\right] = e^{-c\,\delta V} \tag{3.6}$$

This is the van't Hoff entropy approximation[33], valid for $\delta V << V$. Finally, the partition function becomes:

$$Z(f,\beta,c,r,L) = \int \mathcal{D}\left[\hat{\mathbf{t}}(s)\right] e^{-c\,\delta V} \exp\left[-\beta E_{ch}\right] = \int \mathcal{D}\left[\hat{\mathbf{t}}(s)\right] \exp\left[-\beta E_{eff}\right]. \tag{3.7}$$

4 Understanding and calculating the impact of the crowders

In this chapter, we will incorporate the osmotic effects of the crowders in the free energy defined for the pulled Worm-like chain.

4.1 excluded volume due to the polymer and the effective free energy

We consider a semi-flexible polymer (equivalently a WLC), pulled and stretched by an external force f, the polymer is described by its tangent vector $\mathbf{t}(\widehat{\mathbf{s}})$ over the arc length coordinate s spanning the full contour length (L) of the polymer. We assume $\hat{z}$ to be the pulling direction and cylindrical symmetry about the pulling axis.

The effective free energy will have contributions from the bending stiffness with the bare persistence length (A), the coupling of the external pulling force with the polymer extension and an osmotic term which indicates the contribution of the crowders. This osmotic term will simply be the product of the crowder concentration c and the volume excluded to the crowders due to the polymer δV.

$$\beta E = \int_0^L ds \left[\frac{A}{2} (\partial_s \hat{\mathbf{t}})^2 - \beta f \hat{\mathbf{z}} \cdot \hat{\mathbf{t}} \right] + c\,\delta V \tag{4.1}$$

In the zero crowder concentration limit ($c \to 0$, or volume fraction $\phi = vc \to 0$), this equation returns the standard worm-like chain under tension. The model, as described in the previous section, utilises a characteristic force f_c, which is the force on the polymer when the radius of the Pincus blob is the same as the unperturbed persistence length of the polymer. The characteristic force f_c, corresponds to the 50% extension of its maximum length.

For pulling forces $f > f_c$ an expansion of the extension $\langle z \rangle$ gives a full chain extension L, minus a force-dependent term that is proportional to the pulling force.

$$\frac{\langle z \rangle}{L} = 1 - \left(\frac{4f}{f_c} \right)^{-1/2} + ... \tag{4.2}$$

To calculate the δV, we make the first approximation by neglecting any transverse fluctuations of the polymer chain. We assume the polymer to be a rigid rod of radius r_0 and variable elongation z. In this case, the excluded volume, or the volume inaccessible to the crowders, is equal to the volume of a cylinder with radius $R = r_0 + r$ due to the hard-core repulsion. The length of the cylinder will be equal to the extension in the polymer.

$$c\,\delta V\left[\mathbf{t}(\hat{\mathbf{s}})\right] \approx c\,\delta V_{cyl}\left[\mathbf{t}(\hat{\mathbf{s}})\right] = \int_0^L ds\,\pi c R^2\,\hat{\mathbf{t}}\cdot\hat{\mathbf{z}} \tag{4.3}$$

Adding the approximation from (4.3) into (4.1), we get

$$\beta E = \int_0^L ds\,\left[\frac{A}{2}(\partial_s\hat{\mathbf{t}})^2 - \beta f\hat{\mathbf{z}}\cdot\hat{\mathbf{t}}\right] + \int_0^L ds\,\pi c R^2\,\hat{\mathbf{t}}\cdot\hat{\mathbf{z}} \tag{4.4}$$

$$\beta E = \int_0^L ds\,\left[\frac{A}{2}(\partial_s\hat{\mathbf{t}})^2 - \beta\left(f - \frac{\pi c R^2}{\beta}\right)\hat{\mathbf{z}}\cdot\hat{\mathbf{t}}\right] \tag{4.5}$$

This suggests a renormalization of the applied force on the polymer, suggesting that the net effect of the crowders is to counteract the force acted upon the polymer by the external pulling force, which will be discussed later in the results and discussions.

We define a quantity f^* which is,

$$\frac{f^*}{f_c} = \pi c A R^2 = \frac{3}{4}\frac{A}{r}\left(1 + \frac{r_0}{r}\right)^2\phi \tag{4.6}$$

we define a renormalized force $\tilde{f}$ such that,

$$\tilde{f} = f - f^* \tag{4.7}$$

and

$$\frac{\langle z\rangle}{L} = 1 - \left(\frac{f_c}{4\tilde{f}}\right)^{1/2} + ... \tag{4.8}$$

4.2 Incorporating the transverse fluctuations in the excluded volume

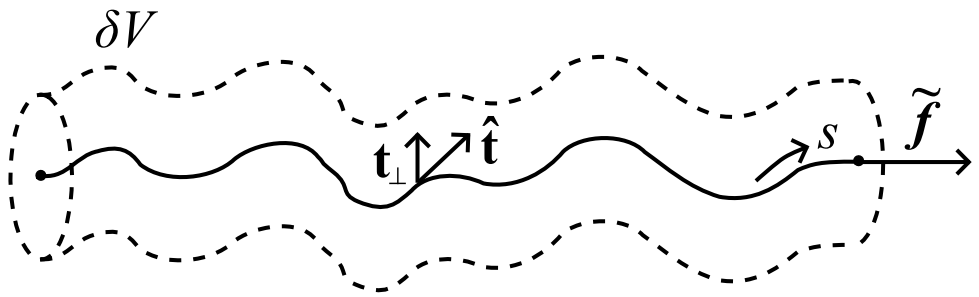

Figure 4.1: An illustration of the fluctuating Worm-Like chain. It represents the crudeness of the solid cylinder approximation of the excluded volume. We can see that, according to this picture, some excluded volume is overestimated or underestimated by the solid cylinder approximation.

In the previous section, we made a very crude approximation by assuming the polymer to be a straight cylinder in the crowder gas. But when the polymer is pulled by an effective force $\tilde{f}$ in the $\hat{\mathbf{z}}$ direction, there are fluctuations in the $\hat{\mathbf{x}}$ and $\hat{\mathbf{y}}$ directions which may change the volume available to the crowders. Thus, it is important to quantify the change in the excluded volume due to these fluctuations and their significance.

The orthogonal displacement of the polymer is given by $\mathbf{u}_\perp(s)$ where

$$\partial_s \mathbf{u}_\perp(s) = \mathbf{t}_\perp(s) \tag{4.9}$$

The fluctuations in $\mathbf{u}_\perp$ have a force-dependent correlation length at any point s_0 along the length of the polymer, given by

$$\langle \mathbf{t}_\perp(s_0) \cdot \mathbf{t}_\perp(s) \rangle = \frac{\xi}{A} \exp\left[-(s - s_0)/\xi\right] \tag{4.10}$$

and

$$\xi = A \left(\frac{f_c}{f}\right)^{1/2} \tag{4.11}$$

Consider a crowder touching the polymer chain at a point s_0, the trajectory of the polymer will act like a rigid rod for all s such that $|s - s_0| < \xi$ and then the trajectory starts acting like a random walk in the transverse direction for $|s - s_0| > \xi$.

4.2.1 Perturbative expansion of the excluded volume

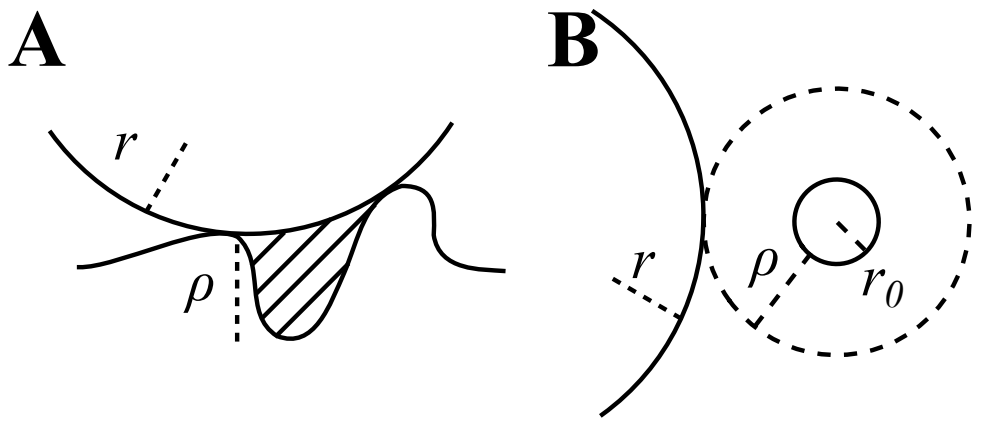

Figure 4.2: (A) Illustrates the polymer trajectory that first comes into contact with the crowder at some s_1 and then the same trajectory touches the crowder at some point s_2 due to the transverse fluctuations. The shaded region represents the additional excluded volume not being accounted for in the solid cylinder approximation. (B) Illustrates the additional fluctuation-dependent radius ρ.

A trajectory will be excluded if it interacts with the crowder again at any other point apart from s_0. To bring this idea into the theory, we consider this effect like an increase in the radius of the depletion cylinder by an extra, fluctuation-dependent radius ρ. It represents the extra volume inaccessible to the crowders.

$$c\,\delta V\left[\hat{\mathbf{t}}(s)\right] \approx \int_0^L ds\,\pi\left(r + r_0 + \rho\right)^2 \tag{4.12}$$

$$c\,\delta V \approx c\,\delta V_{cyl} + \pi\left[\langle\rho^2\rangle + 2R\sqrt{\langle\rho^2\rangle}\right] \tag{4.13}$$

4.2.2 Calculation of $\langle \rho^2 \rangle$

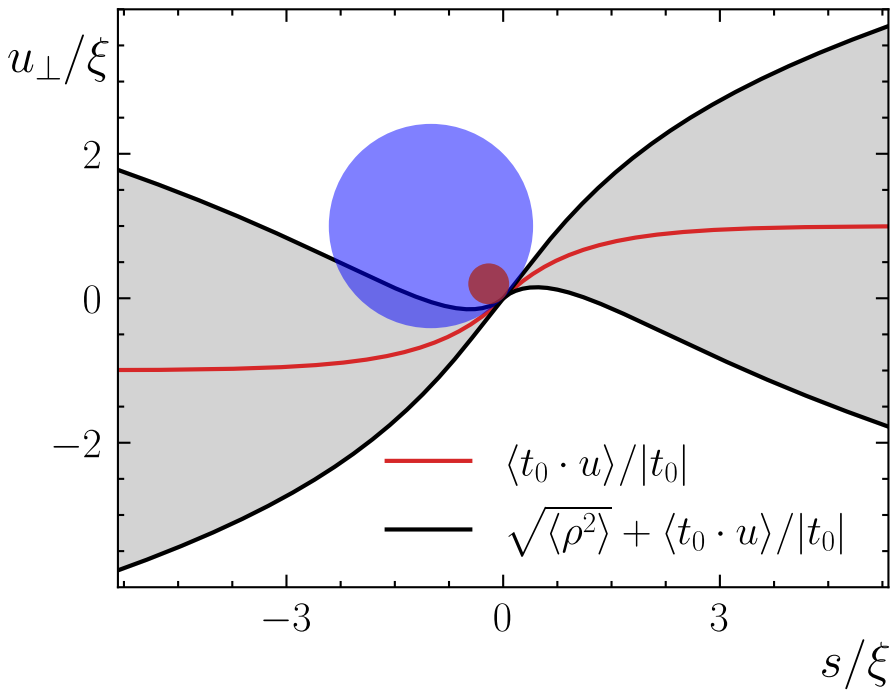

Figure 4.3: A 1D illustration of the calculation for $\langle \rho^2 \rangle$ at a fixed r/r_0 and ϕ. It represents two spherical crowders of different radii touching the polymer at $s = 0$. It shows that the non-zero mean component(red solid line) of the WLC trajectory along the component of $\mathbf{t}_\perp(0)$ direction does not contribute to the depletion, whereas the standard deviation does(grey shaded region).

In the equation (4.13), the calculation of $\langle \rho^2 \rangle$ poses a significant challenge. To calculate this, we first considered the orthogonal displacement $\mathbf{u}_\perp(s)$ of the WLC conformation over distances comparable to the size of the crowders (r), which should be compared to the correlation length for bending and displacement fluctuations ξ.

For a particular trajectory, care must be taken while the crowder size r is less than the correlation length ξ of the fluctuations. As in this regime, the strong correlation of the tangent vector comes into play over the distances of the crowder size. We represent the correlated length at a particular segment by $\langle \mathbf{t}_\perp(\mathbf{0}) \cdot \mathbf{u}_\perp(\mathbf{s}) \rangle / \langle |\mathbf{t}_\perp(\mathbf{0})|^2 \rangle^{1/2}$. It is a nonzero quantity that represents the component of orthogonal displacement in the direction of the tangent vector tilt, $\mathbf{u}_\perp(\mathbf{0})/|\mathbf{u}_\perp(\mathbf{s})|$ i.e. the unit tangent vector at the point of contact.

The projection can be calculated as following:

$$\frac{\mathbf{t}_\perp(\mathbf{0}) \cdot \mathbf{u}_\perp(\mathbf{s}) \rangle}{\langle |\mathbf{t}_\perp(\mathbf{0})|^2 \rangle^{1/2}} = \int_0^r ds \, \frac{\mathbf{t}_\perp(\mathbf{0}) \cdot \mathbf{t}_\perp(\mathbf{s}) \rangle}{\langle |\mathbf{t}_\perp(\mathbf{0})|^2 \rangle^{1/2}} = \left(\frac{\tilde{f}}{f_c} \right)^{1/4} \xi \left(1 - e^{-s/\xi} \right) \tag{4.14}$$

Subtracting this projection from $u_\perp(s)$ yields the correct transverse volume, as now we are looking at the displacement fluctuation in the tilted reference frame. With this,

the fluctuation-corrected radius, as a function of r, now becomes,

$$\langle \rho^2 \rangle = \left\langle \left| \mathbf{u}_\perp(r) - \frac{\langle \mathbf{t}_\perp(0) \cdot \mathbf{u}_\perp(r) \rangle \mathbf{t}_\perp(0)}{\langle |\mathbf{t}_\perp(0)|^2 \rangle} \right|^2 \right\rangle, \tag{4.15}$$

Solving the equation by squaring, the cross terms will vanish, and we are left with

$$\langle \rho^2 \rangle = \int_0^r ds \int_0^r ds' \langle \mathbf{t}_\perp(\mathbf{s}) \cdot \mathbf{t}_\perp(\mathbf{s}') \rangle - \left(\int_0^r \mathrm{d}s \, \frac{\langle \mathbf{t}_\perp(0) \cdot \mathbf{t}_\perp(s) \rangle}{\langle |\mathbf{t}_\perp(0)|^2 \rangle^{1/2}} \right)^2 \tag{4.16}$$

Now we just take the equation (4.16) and solve each integral individually using the following relation. The integration is simple, and a standard technique.

$$\langle t_\perp(s).t_\perp(0) \rangle = \frac{\xi}{A} \, e^{-(s/\xi)} \tag{4.17}$$

$$\begin{aligned} I_1 &= \int_0^r ds \int_0^r ds' \, \langle t_\perp(s).t_\perp(s') \rangle \\ &= \frac{\xi}{A} \int_0^r ds \int_0^r ds' \, e^{-|s-s'|/\xi} \\ &= \frac{\xi}{A} \xi^2 \int_0^\lambda dx \int_0^\lambda dx' e^{-|x-x'|} \qquad \text{with} \qquad \lambda = \frac{r}{\xi} \\ &= \frac{2\xi^3}{A} \int_0^\lambda dx \; e^{-x} \int_0^x dx' e^{x'} \\ &= \frac{2\xi^3}{A} \left(e^{-\lambda} - 1 + \lambda \right) \end{aligned} \tag{4.18}$$

$$\begin{aligned} I_2 &= \left(\int_0^r ds \frac{\langle \mathbf{t}_\perp(0) \cdot \mathbf{t}_\perp(0) \mathbf{t}_\perp(0) \rangle}{\langle |\mathbf{t}_\perp(0)|^2 \rangle} \right)^2 \\ &= \int_0^r ds \frac{\langle \mathbf{t}_\perp(0) \cdot \mathbf{t}_\perp(0) \rangle^2}{\langle |\mathbf{t}_\perp(0)|^2 \rangle} \\ &= \frac{\xi^3}{A} \left(\int_0^\lambda dx \, e^{-x} \right)^2 \qquad \text{with} \qquad \lambda = \frac{r}{\xi} \\ &= \frac{\xi^3}{A} \left(1 - e^{-\lambda} \right)^2 \end{aligned}$$

Putting I_1 and I_2 together in the equation (4.16) we get,

$$\langle \rho^2 \rangle = \frac{\xi^3}{A} g(\lambda), \quad \text{where} \quad g(\lambda) = 2\lambda - 3 + 4e^{-\lambda} - e^{-2\lambda}. \tag{4.19}$$

So the fluctuation-dependent radius of the cylinder is a function of ξ and λ, where $\xi = A\sqrt{f_c/\tilde{f}}$ is the force-dependent persistence length of the polymer from the Marko-

Siggia WLC theory and carries a similar meaning as here it has the normalized force in the denominator. And we have $\lambda = r/\xi$, that is, the relative crowder size with respect to the apparent persistence length. This quantity will become relevant when we want to understand the significance of transverse fluctuations with respect to crowder size.

4.3 Deriving the force Extension relation

Finally, we can calculate the force-extension relationship by using a simple formula:

$$\frac{\langle z \rangle}{L} = -\frac{\partial\, ln(Z)}{\partial \beta f} \tag{4.20}$$

Through the canonical ensemble, we obtain

$$\frac{1}{L}\ln Z = \beta\tilde{f} - \sqrt{\frac{\beta\tilde{f}}{A}} - \pi c\left(2R\sqrt{\langle\rho^2\rangle} + \langle\rho^2\rangle\right) + O\left(\tilde{f}^{-3/2}\right) \tag{4.21}$$

4.3.1 Force-extension relationship in the absence of transverse fluctuations

$$\frac{\langle z \rangle}{L} = 1 - \sqrt{\frac{f_c}{4\tilde{f}}} \tag{4.22}$$

4.3.2 Force extension relationship in presence of transverse fluctuations

$$\frac{1}{L}\log Z\left(\lambda, \xi, A\right) = \beta\tilde{f} - \sqrt{\beta\tilde{f}/A} - \pi c\left(\left\langle\rho^2\right\rangle + 2R\sqrt{\langle\rho^2\rangle}\right) + \mathcal{O}(\tilde{f}^{-3/2}), \tag{4.23}$$

The force-extension relationship follows as $\langle z\rangle/L = \partial \log Z/\partial(\beta\tilde{f})$, leading to correction of the zeroth-order force extension relationship of Eq. **??**

$$\frac{1}{L}\ln Z = \beta\tilde{f} - \pi c\left(2R\sqrt{\frac{\xi^3}{A}\left(2\lambda - 3 + 4e^{-\lambda} - e^{-2\lambda}\right)}\right. \tag{4.24}$$

$$\left. + \frac{\xi^3}{A}\left(2\lambda - 3 + 4e^{-\lambda} - e^{-2\lambda}\right) - \sqrt{\frac{\beta\tilde{f}}{A}} + O\left(\tilde{f}^{-3/2}\right)\right. \tag{4.25}$$

$$\frac{1}{L}\frac{\partial \ln Z}{\partial \beta f} = 1 - \frac{\xi}{2A} - \pi c \Bigg(\frac{-3R\,\xi^{7/2}}{2A^{3/2}} \left(2\lambda - 3 + 4e^{-\lambda} - e^{-2\lambda}\right)^{1/2} + \frac{Rr\,\xi^{5/2}}{2A^{3/2}} \frac{2 - 4e^{-\lambda} + 2e^{-2\lambda}}{\left(2\lambda - 3 + 4e^{-\lambda} - e^{-2\lambda}\right)^{1/2}} + \frac{-3\,\xi^{5}}{2A^{2}} \left(2\lambda - 3 + 4e^{-\lambda} - e^{-2\lambda}\right) + \frac{r\,\xi^{4}}{2A^{2}} \left(2 - 4e^{-\lambda} + 2e^{-2\lambda}\right) \Bigg) \tag{4.26}$$

The above equation can be condensed into a more compact one which makes understanding it's nuances and further analysis much more easy.

$$\frac{\langle z \rangle}{L} = \frac{z_0}{L} + \frac{3\phi}{8} \left[\frac{\xi^2}{A^2} + \frac{(r_0 + \lambda\xi)\,\xi^{1/2}}{\sqrt{g(\lambda)}A^{3/2}} \right] \frac{3g(\lambda) - \lambda g'(\lambda)}{\lambda^3}, \tag{4.27}$$

Here $(z_0/L = 1 - (f_c/[4\tilde{f}])^{1/2})$ and ϕ, ξ, λ, $g(\lambda)$ all carry their usual meanings.

5 Results

In this chapter, we will go over some of the key results of this research. The chapter is structured such that we first discuss the impact of our considerations in calculating the excluded volume δV on the force extension relationship as derived in equations (4.22), and (4.27). We will also do an asymptotic analysis of the eq. (4.27) to ensure that our model is in line with the previously proposed model and then point out some interesting phenomenology that we observe.

5.1 The Osmotic force has a compacting effect on the polymer in the Zeroth order

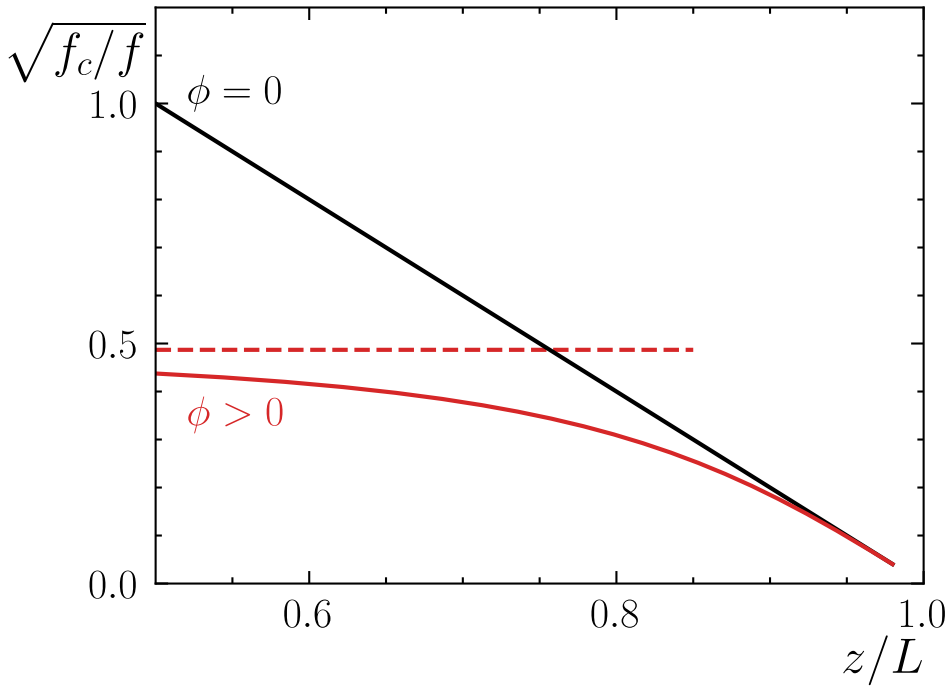

Figure 5.1: Force-extension relationship without crowders(in black) vs with crowders(in red). The dashed line represents the compaction force f^* applied by the crowders on the polymer as per eq. (4.6)

To understand the impact of crowders on the polymer chain, we made a simplistic approximation of the polymer-crowder system. We assumed that the polymer acted as a rigid cylinder, ignoring any transverse fluctuations, and the volume inaccessible to the crowders is a cylinder of radius $R = r_0 + r$.

This zeroth-order approximation predicted that the osmotic force on the polymer due to the crowders counteracts the extension force f acting on the polymer with a dependence on the conformation $\hat{\mathbf{t}}$ as the pulling term (see eq. (4.5)). This results an effective reduction in the pulling force by a crowder dependent force f^* as depicted in the figure with the red line.

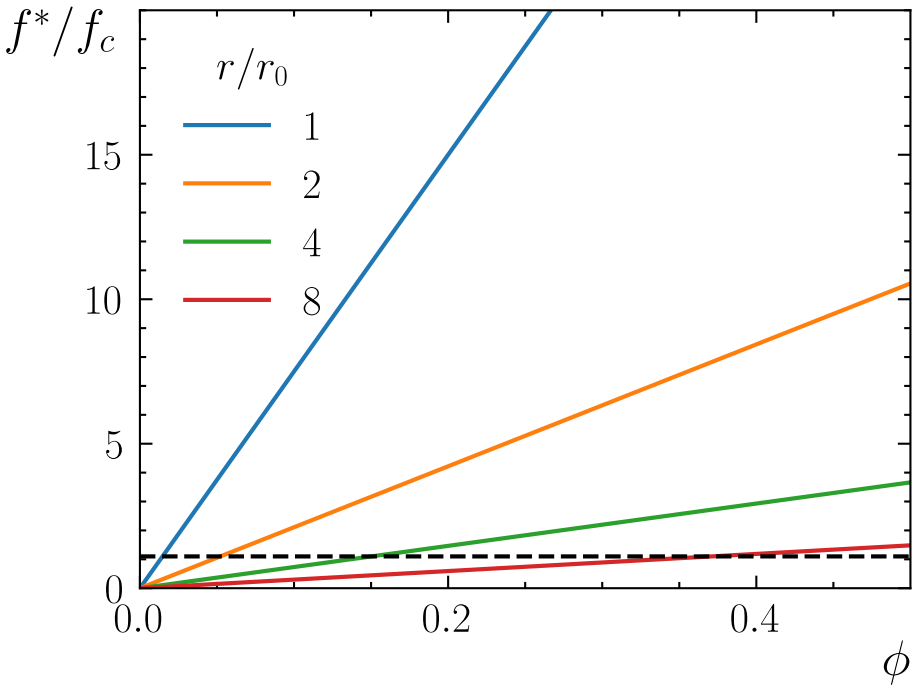

Figure 5.2: Collapse force f^* as a function of ϕ and relative crowder size r/r_0. This shows that the collapse force increases for smaller crowders. The dashed line in the figure corresponds to $f^* = 1.1 f_c$. Below this line the collapsing effect is very small.

The crowder-dependent compaction force f^* (see eq. (4.6)) is a function of the crowder size relative to the monomer size r_0/r and the volume fraction. As shown in the figure Figure, we observe that for a constant crowder fraction ϕ smaller crowders apply a higher compacting force as compared to the bigger crowders. This is a result of the crowding force being an osmotic pressure phenomenon. In simple terms, the polymer experiences a higher force when it has more crowders coming in contact with its surface. As the crowders get bigger, fewer crowders can exist in the same volume thus reducing the force experienced by the polymer.

5.2 The Transverse fluctuations tend to swell the polymer

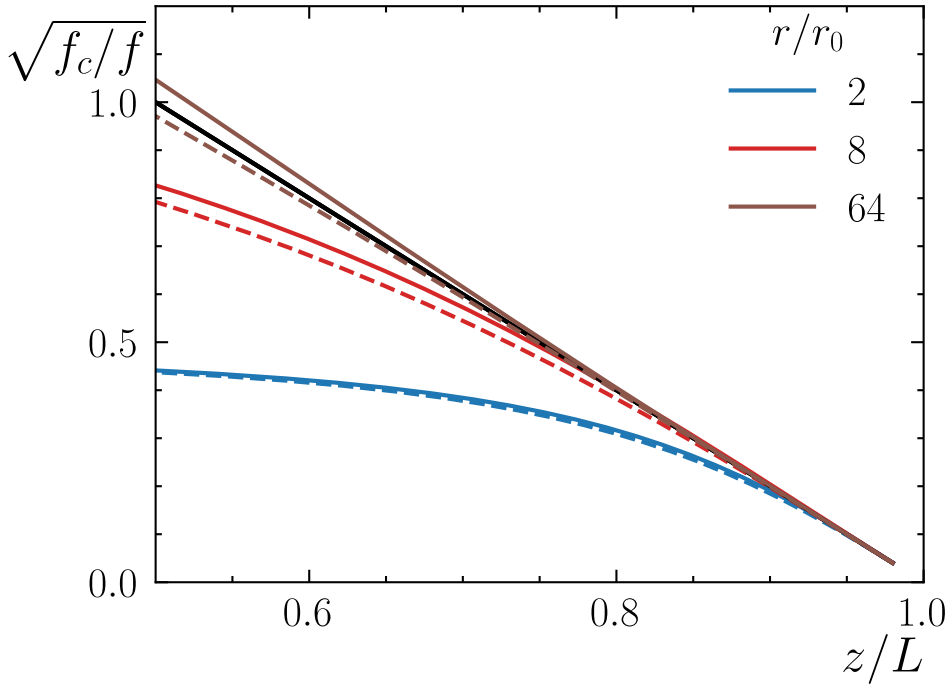

Figure 5.3: The figure depicts the effect of the transverse fluctuations on the force-extension relationship for different relative crowder sizes r/r_0. The dashed line depicts the zeroth-order effect that compacts the polymer, and the solid line represents the second-order correction, which counteracts the compaction and is actually swelling in nature.

As discussed in the previous section, the zeroth-order approximation predicts a compacting effect by the crowders on the polymer. The addition of transverse fluctuations shows a more nuanced behaviour for the force-extension that depends on the relative size of the crowder (r/r_0) and the force-dependent persistence length.

The solid black line in the Fig. 5.3 represents the force-extension relationship from the Marko-Siggia theory of WLC under stretching in zero crowder condition ($\phi = 0$) as in Fig. 2.2. The dashed lines in Fig. 5.3 are the zeroth-order correction as in Fig. 5.1, and the solid lines show the force-extension with transverse fluctuations as a function of r/r_0 and λ as per the eq. (4.2) and eq. (4.27).

The figure shows that, first, the second-order correction has a swelling nature regardless of the crowder size. And that the crowder size plays a critical role in the relevance of the transverse fluctuations. As the correction is almost negligible for small crowder size ($r/r_0 = 2$) in blue. But as we increase the relative crowder size, the swelling effect becomes more and more relevant (red and brown curves).

5.3 Asymptotic behaviour of $g(\lambda)$ and the force extension relationship

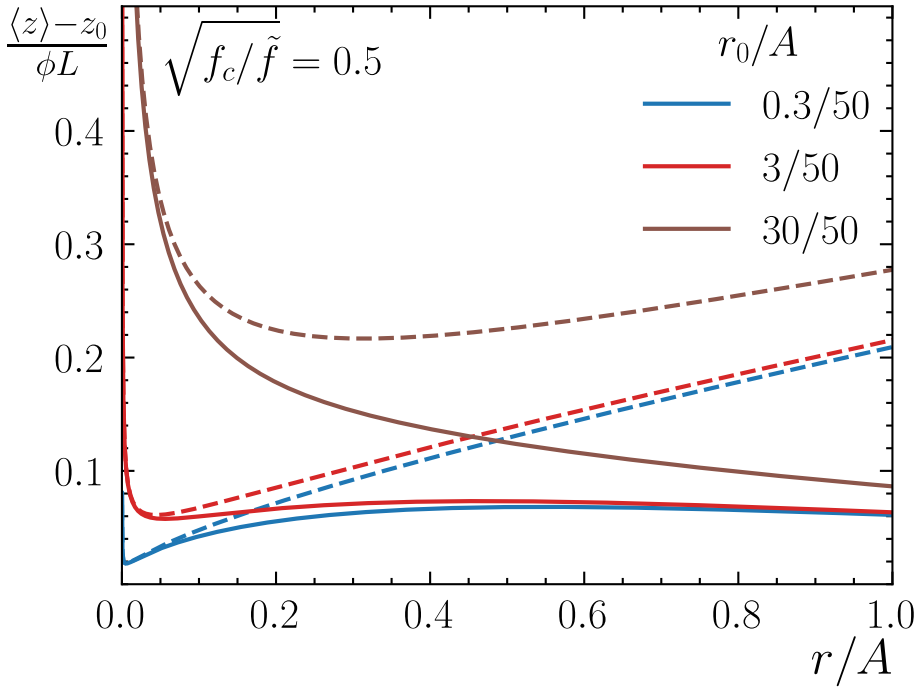

Figure 5.4: This figure highlights the polymer fluctuation-dependent contribution to the force extension as a function of r/A at a fixed effective force ($\sqrt{f_c/\tilde{f}} = 0.5$). The solid lines represent the contribution for various monomer sizes relative to the bare persistence lengths. The dashed lines represent the behaviour for $\lambda << 1$

We can rewrite equation (4.27) as:

$$\frac{\langle z\rangle - z_0}{L\phi} = \frac{3}{8}\left[\frac{\xi^2}{A^2} + \frac{(r_0+\lambda\xi)\,\xi^{1/2}}{\sqrt{g(\lambda)}A^{3/2}}\right]\frac{3g(\lambda) - \lambda g'(\lambda)}{\lambda^3} \tag{5.1}$$

For sufficiently high forces and large crowders ($r > \xi \quad \text{or} \quad \lambda > 1$); $g(\lambda = 2\lambda + \cdots$, with $\langle\rho^2\rangle = 2\xi^2/A + \cdots$ in its asymptotic limit, which is compatible with the predictions of regular WLC in its high force regime[32].

On the other hand, when the crowder is small, ($r < \xi$ or $\lambda < 1$) , $g(\lambda) = 2r^3/3A$. This means in the small crowder or the small λ limit, the force dependence of the fluctuation radius disappears, which is compatible with the analysis of transverse fluctuations of WLC under confinement as shown in [34]. This is a very important result as we could not have achieved the right small-λ behavior if we had not removed the tangent tilt. without removing the tangent tilt, $g(\lambda) \approx \lambda^2$ and $\langle\rho^2\rangle \approx r^2\xi/A$, resulting in unrealistic force dependence of even in the absence of crowders or $r \to 0$.

following the analysis of $g(\lambda)$. We can now concentrate on (5.1), whose results are represented in 5.4. We immediately notice that the fluctuation correction to $\langle z/L$ in (4.27) will always be positive as the term $3g(\lambda) - \lambda g'(\lambda)$ positive for all λ and all other quantities can only be positive. Following this, we define a new characteristic force f_λ which is the force($\tilde{f}$) at which the $\lambda = 1$ or $r = \xi$ which also marks the boundary between the two fluctuation regimes.

First, we look at fluctuation contribution when $f_\lambda << \tilde{f}$ i.e. when the applied force is much larger than the characteristic force. In this case, the fluctuation correction goes to zero as $O[(f_c/\tilde{f})^{3/2}]$ asymptotically. This physically makes sense, as at very high forces, the polymer approaches the contour length. The fluctuation contribution also decreases for very large crowders as $O[(A/r)^{3/2}]$.

In the other regime, $f_\lambda >> \tilde{f}$, , i.e. when the applied force is less than the characteristic force, $g(\lambda) \approx 2\lambda^3/3$ and $g(\lambda) - \lambda g'(\lambda) \approx \lambda^4/2$, which leads to the fluctuation correction looking like

$$\frac{\langle z\rangle - z_0}{L\phi} \simeq \frac{3}{16}\left[\frac{r}{A} + \sqrt{\frac{3}{2}}\left(\frac{r}{A} + \frac{r_0}{A}\right)\sqrt{\frac{A}{r}}\right]\sqrt{\frac{f_c}{\tilde{f}}}. \tag{5.2}$$

The contribution from the fluctuation correction varies as $\sqrt{f_c/\tilde{f}}$ which is the same as the variation in a z_0/L as in eq. (5.1). So at small forces, the fluctuation correction would appear like the polymer has a persistence length different from the bare persistence length A. The bulkier is the polymer, the greater the contribution from fluctuations. Also, as a function of r/A the function has a minimum at $r \approx r_0$ and it increases for larger r/A.

At fixed external force $\tilde{f}/f_c$, the eq. (5.1) has a maximum for $r \approx \xi$, when the radius of the crowder is almost equal to the force-dependent persistence length of the polymer, but this only holds in the regime when $r_0/A << \sqrt{f_c/\tilde{f}}$ or when the polymer is slender enough as is visible in the fig. 5.4. Our result also implies that at high enough forces, small crowders tend to have higher swelling contribution compared to the larger crowders, but in absolute terms, the effect is just too small to be visible in the figure 5.4.

6 Discussion

The central outcome of this research is that neutral crowders, who have a purely steric interaction with the polymer, can modify the mechanical response of a semiflexible polymer. It was previously understood and theorized that neutral crowders only have a compacting effect on the polymer. But our theory suggests that the effect is not purely compacting but is tuned by the size of the crowder. While steric exclusion generates a compacting osmotic force, transverse fluctuations have a fluctuation-induced swelling effect which counters the compaction. The interplay of these two effects produces a rich force-extension behaviour.

As shown in the theory and the results, neutral crowders with purely steric interactions with the polymer can tune the mechanical response of a semi-flexible polymer under tension. Previously, it was shown experimentally and through simulations that the crowders only had a compacting effect, irrespective of the crowder size and volume fraction. Our results explicitly show that consideration of only steric effects generates a compacting osmotic force, but incorporating transverse fluctuations makes the resultant mechanical response more sensitive to the relative size of the crowder (r/r_0) and the volume fraction of the crowder (ϕ), leading to a competition between osmotic compaction and fluctuation-driven swelling of the polymer.

At leading order, the excluded volume between the polymer and the crowders acts as an effective additive force opposing the externally applied extension force. This compacting force scales like

$$f^* \approx k_B T \frac{\phi}{r} \tag{6.1}$$

The simplest physical interpretation of this osmotic force could be the osmotic pressure of the crowders acting over a cross-sectional area of interaction between the polymer and the crowder. For large enough f^*, the compacting force may even drive the polymer to a collapsed state even in the presence of an extending force($\tilde{f} \leq 0$).

But, the transverse fluctuations in the polymer significantly alter the excluded volume. Because bending fluctuations effectively increase the spatial volume unavailable to the crowders, the correction term introduced has a swelling effect on the force-extension curve. This swelling can be understood as an attempt by the system to reduce its free energy by allowing the polymer to extend a little, reducing the overlap between the fluctuating

segments and the surrounding crowders. But this fluctuation-dependent swelling term is sensitive to the crowder size and applied force.

Putting both the compacting effects of the leading order approximation of the excluded volume and the swelling effect of the fluctuation-driven second order correction gives rise to three regimes of the force-extension relationship.

(i) If the crowders are very small, or the crowder volume fraction (ϕ) is very large, the polymer response is dominated by the osmotic compaction of the crowders.

(ii) If the ϕ is small enough such that $f^* < f_c$ and the crowder size is large enough such that the transverse fluctuations stay relevant. In that case, the theory predicts a counterintuitive swelling of the polymer due to the crowders. The crowders can even drive the extension beyond the uncrowded regime force extension. This behaviour is depicted by the brown curve in Fig. 5.3. And finally,

(iii) If the tension is extremely large, i.e. the strong stretching regime, the extension approaches the contour length of the polymer and the polymer is now in the rigid rod limit where the fluctuation-dependent swelling becomes negligible.

These three regimes can be interpreted as different regions of an effective parameter space spanned by a dimensionless force, crowder size ratio r/r_0, and volume fraction ϕ. The crossover from the compaction-dominated regime to the fluctuation-dominated regime can be understood as a phase boundary analogous to a polymer collapse transition.

The theory can serve as a tool to understand DNA compaction *in vivo* and other intracellular polymer compaction processes. Beyond providing a simple qualitative understanding, one can also make testable predictions using our results.

Our theory, even in its present simple form, can directly inform single-molecule pulling experiments. Quantitatively, the theory predicts a force renormalization of order $f^* \sim k_B T\phi/r$, which for typical experimental conditions ($\phi \sim 0.1$, $r \sim 1 - 10\,\text{nm}$) corresponds to forces in the sub-piconewton to piconewton range. We predict that the addition of crowders normalizes the force, and the force read by the instrument is not the one experienced by the polymer under stretching. We believe that the addition of crowders would lead to a shift up in cantilever-type experiments that use constant extension, and a shift down in the apparent force in experiments that use constant force methods. Experiments that use fluctuations (e.g., magnetic tweezers [23, 27, 32, 34–36]) to calibrate can also benefit from our theory, as at a constant external force, an addition of crowders leads to enhanced transverse fluctuations as predicted by the theory.

The predicted competition between the osmotic compaction and fluctuation-induced swelling suggests that experiments should be designed to systematically vary both the crowder size (r) and the volume fraction (ϕ). The theory identifies a non-trivial regime of polymer swelling with large and dilute crowders. Observing this effect is challenging, but controlled variation in crowder size at fixed volume fraction, using well-characterized polymeric crowders such as PEG could be useful.

The theory highlights the relevance of transverse fluctuations in determining the mechanical response of polymers. This information can be used to test a new set of experimental observables, like fluctuation spectra and extension variance, which can contain additional information about the crowding effects. Furthermore, the theory allows for an inverse characterization of the crowded environments: By fitting the force-extension data obtained in an unknown crowding environment to the theoretical predictions. This can be used to extract effective parameters, such as crowder size and volume fraction. In this sense, the theory can then serve as a mean-field description for the system, allowing complex and heterogeneous crowding conditions to be mapped onto an effective coarse-grained representation.

We have made several assumptions while making this theory, and one should be careful when comparing with experimental data. We compute the osmotic pressure assuming a dilute system of crowders where the ideal gas approximation is valid. The worm-like chain effective energy was expanded using a perturbation expansion in the strong stretching limit, where we assumed the fluctuations to be small and Gaussian distributed. on top of that we have also neglected higher order virial coefficients, many-body correlations, polymer self-avoidance and hydrodynamics drag effects. These approximations may constrain the quantitative validity of the model at high crowder volume fractions as in typical cellular environments.

To make this theory more realistic, a natural extension would incorporate non-ideal crowder equations of state, such as the Carnahan-Starling approximation equation. The crowder environment inside the cell is not uniform and contains many different kinds of crowders, which simultaneously interact with the DNA, thus it would be interesting to see the effects of polydispersity in this theory. One can also look into the statistics of the crowding-induced collapsed globule as predicted by this theory in the $\tilde{f} < 0$ regime. Extensions to active or non-equilibrium crowders may also provide some insights towards modelling the effects of molecular motors and other active machinery within the cell[37].

Despite our simplification, the present theory provides predictive insights into how steric crowding modifies the behaviour of a semiflexible polymer under a broad range of forces. By linking the microscopic excluded volume with the macroscopic elasticity of the polymer, our theory offers a framework to better interpret force spectroscopy datasets and enhances our understanding of chromosome compaction in intracellular environments.

7 Conclusion

This thesis successfully derives an analytical relationship between purely steric macromolecular crowding interactions with a semi-flexible polymer and its mechanical response. We developed an effective free energy in the Gibbs ensemble by incorporating the excluded volume effects of the crowder polymer system and the bending fluctuations of the polymer.

We first approximated the volume inaccessible to the crowders due to the polymer as a solid cylinder, assuming a simple hard-core repulsion between the two. Within this approximation, we showed that monodisperse spherical crowders exert a uniform compacting force on the polymer under tension, opposing the external. This force by the crowders also normalizes the free energy and the force-extension relationship.

We also investigated the effects of bending fluctuations in the strong stretching ($\langle z \rangle / L > 0.5$) limit through a perturbation expansion, assuming a force-dependent fluctuation radius. In this limit, we showed that fluctuations have a swelling effect counteracting the compaction of the osmotic pressure. And we predicted a parameter range in which our novel swelling could be of significance.

With this work, we were able to bridge the gap between microscopic steric interactions and macroscopic elasticity of semi-flexible polymer. In the strong stretching and dilute crowder regime, this theory offers predictive power across a broad range of physiological forces, therefore aiding the interpretation of single-molecule force spectroscopy experiments in crowded environments.

Although we make several approximations to simplify the problem, the theory offers a firm base for future extensions to the theory, like incorporating non-ideal equations of state [38], heterogeneous crowding or active crowders, enabling future studies with more realistic intracellular environments.

In conclusion, this thesis presents an analytical theory to show that macromolecular crowding is not just a passive confinement, but it takes an active role in tuning the macroscopic mechanical response of the polymer under tension, enhancing our understanding of biological systems.

Bibliography

[1] Mirjana Macvanin and Sankar Adhya. Architectural organization in e. coli nucleoid. *Biochimica et Biophysica Acta*, 2012. doi: 10.1016/J.BBAGRM.2012.02.012.

[2] Subhash Verma, Qian Zhong, and Sankar Adhya. Architecture of the escherichia coli nucleoid. *PLoS Genetics*, 2019. doi: 10.1371/JOURNAL.PGEN.1008456.

[3] Vladimir B. Teif and Klemen Bohinc. Condensed DNA: Condensing the concepts. *Progress in Biophysics and Molecular Biology*, 105(3):208–222, May 2011. ISSN 00796107. doi: 10.1016/j.pbiomolbio.2010.07.002. URL https://linkinghub.elsevier.com/retrieve/pii/S0079610710000659.

[4] Michèle Valens, Stéphanie Penaud, Michèle Rossignol, François Cornet, and Frédéric Boccard. Macrodomain organization of the Escherichia coli chromosome. *The EMBO Journal*, 23(21):4330–4341, October 2004. ISSN 1460-2075. doi: 10.1038/sj.emboj.7600434. URL https://doi.org/10.1038/sj.emboj.7600434.

[5] Lisa Postow, Christine D. Hardy, Javier Arsuaga, and Nicholas R. Cozzarelli. Topological domain structure of the Escherichia coli chromosome. *Genes & Development*, 18(14):1766–1779, July 2004. ISSN 0890-9369, 1549-5477. doi: 10.1101/gad.1207504.

[6] Martijn S. Luijsterburg, Maarten C. Noom, Gijs J. L. Wuite, and Remus Th. Dame. The architectural role of nucleoid-associated proteins in the organization of bacterial chromatin: A molecular perspective. *Journal of Structural Biology*, 156(2):262–272, November 2006. ISSN 1047-8477. doi: 10.1016/j.jsb.2006.05.006.

[7] Shane C. Dillon and Charles J. Dorman. Bacterial nucleoid-associated proteins, nucleoid structure and gene expression. *Nature Reviews Microbiology*, 8(3):185–195, March 2010. ISSN 1740-1534. doi: 10.1038/nrmicro2261. URL https://www.nature.com/articles/nrmicro2261.

[8] Sravani Keerthi Ramisetty and Rita S. Dias. Synergistic role of DNA-binding protein and macromolecular crowding on DNA condensation. An experimental and theoretical approach. *Journal of Molecular Liquids*, 210:64–73, October 2015.

ISSN 01677322. doi: 10.1016/j.molliq.2015.04.051. URL https://linkinghub.elsevier.com/retrieve/pii/S016773221530060X.

[9] James J. Champoux. Dna topoisomerases: structure, function, and mechanism. *Annual review of biochemistry*, 2001. doi: 10.1146/ANNUREV.BIOCHEM.70.1.369.

[10] Tatyana Romantsov, Itzhak Fishov, and Oleg Krichevsky. Internal structure and dynamics of isolated escherichia coli nucleoids assessed by fluorescence correlation spectroscopy. *Biophysical journal*, 2007. doi: 10.1529/BIOPHYSJ.106.095729.

[11] Romain Rollin, Jean-François Joanny, and Pierre Sens. Physical basis of the cell size scaling laws. *eLife*, 12:e82490, May 2023. ISSN 2050-084X. doi: 10.7554/eLife.82490.

[12] Theo Odijk. Osmotic compaction of supercoiled DNA into a bacterial nucleoid. *Biophysical Chemistry*, 73(1):23–29, July 1998. ISSN 0301-4622. doi: 10.1016/S0301-4622(98)00115-X.

[13] Vincenzo G. Benza, Bruno Bassetti, Kevin D. Dorfman, Vittore F. Scolari, Krystyna Bromek, Pietro Cicuta, and Marco Cosentino Lagomarsino. Physical descriptions of the bacterial nucleoid at large scales, and their biological implications. *Reports on Progress in Physics. Physical Society (Great Britain)*, 75(7):076602, July 2012. ISSN 1361-6633. doi: 10.1088/0034-4885/75/7/076602.

[14] Sho Asakura and Fumio Oosawa. On Interaction between Two Bodies Immersed in a Solution of Macromolecules. *The Journal of Chemical Physics*, 22(7):1255–1256, July 1954. ISSN 0021-9606, 1089-7690. doi: 10.1063/1.1740347. URL http://aip.scitation.org/doi/10.1063/1.1740347.

[15] C Robinow and E Kellenberger. The bacterial nucleoid revisited. *Microbiological Reviews*, 58(2):211–232, June 1994. ISSN 0146-0749. doi: 10.1128/mr.58.2.211-232.1994. URL https://pmc.ncbi.nlm.nih.gov/articles/PMC372962/.

[16] Michael Rubinstein. *Polymer Physics*. Oxford University Press, 2003. ISBN 978-1-61344-943-1. Google-Books-ID: EJrYoAEACAAJ.

[17] Alexander Yu Grosberg, Alexei R. Khokhlov, and H. Eugene Stanley. *Statistical Physics of Macromolecules*. Polymers and Complex Materials. AIP-Press, 1994. ISBN 978-1-56396-071-0.

[18] Paul J. Flory. *Principles of Polymer Chemistry*. Cornell University Press, 1953. ISBN 978-0-8014-0134-3. Google-Books-ID: CQ0EbEkT5R0C.

[19] P.G. De Gennes. Collapse of a polymer chain in poor solvents. *Journal de Physique Lettres*, 36(3):55–57, 1975. ISSN 0302-072X. doi: 10.

1051/jphyslet:0197500360305500. URL http://www.edpsciences.org/10.1051/jphyslet:0197500360305500.

[20] L. S. Lerman. A Transition to a Compact Form of DNA in Polymer Solutions. *Proceedings of the National Academy of Sciences of the United States of America*, 68(8):1886–1890, 1971. ISSN 0027-8424. URL https://www.jstor.org/stable/61306.

[21] Carlos J. Bustamante, Yann R. Chemla, Shixin Liu, and Michelle D. Wang. Optical tweezers in single-molecule biophysics. *Nature Reviews Methods Primers*, 1(1):25, March 2021. ISSN 2662-8449. doi: 10.1038/s43586-021-00021-6. URL https://www.nature.com/articles/s43586-021-00021-6.

[22] Da Yang, Jaana Männik, Scott T. Retterer, and Jaan Männik. The effects of polydisperse crowders on the compaction of the *Escherichia coli* nucleoid. *Molecular Microbiology*, 113(5):1022–1037, May 2020. ISSN 0950-382X, 1365-2958. doi: 10.1111/mmi.14467. URL https://onlinelibrary.wiley.com/doi/10.1111/mmi.14467.

[23] M. Cristofalo, C. A. Marrano, D. Salerno, R. Corti, V. Cassina, A. Mammola, M. Gherardi, B. Sclavi, M. Cosentino Lagomarsino, and F. Mantegazza. Cooperative effects on the compaction of DNA fragments by the nucleoid protein H-NS and the crowding agent PEG probed by Magnetic Tweezers. *Biochimica et Biophysica Acta (BBA) - General Subjects*, 1864(12):129725, December 2020. ISSN 0304-4165. doi: 10.1016/j.bbagen.2020.129725.

[24] Shiori Iida, Satoru Ide, Sachiko Tamura, Masaki Sasai, Tomomi Tani, Tatsuhiko Goto, Michael Shribak, and Kazuhiro Maeshima. Orientation-independent-DIC imaging reveals that a transient rise in depletion attraction contributes to mitotic chromosome condensation. *Proc Natl Acad Sci U S A*, 121(36):e2403153121, September 2024. doi: 10.1073/pnas.2403153121.

[25] James Pelletier, Ken Halvorsen, Bae-Yeun Ha, Raffaella Paparcone, Steven J. Sandler, Conrad L. Woldringh, Wesley P. Wong, and Suckjoon Jun. Physical manipulation of the Escherichia coli chromosome reveals its soft nature. *Proceedings of the National Academy of Sciences*, 109(40):E2649–E2656, October 2012. doi: 10.1073/pnas.1208689109.

[26] Andreia F. Jorge, Sandra C.C. Nunes, Tânia F.G.G. Cova, and Alberto A.C.C. Pais. Cooperative action in DNA condensation. *Current Opinion in Colloid & Interface Science*, 26:66–74, December 2016. ISSN 13590294. doi: 10.1016/j.cocis.2016.09.014. URL https://linkinghub.elsevier.com/retrieve/pii/S1359029416301467.

[27] Andrea Soranno, Iwo Koenig, Madeleine B. Borgia, Hagen Hofmann, Franziska Zosel, Daniel Nettels, and Benjamin Schuler. Single-molecule spectroscopy reveals polymer effects of disordered proteins in crowded environments. *Proceedings of the National Academy of Sciences of the United States of America*, 111(13):4874–4879, April 2014. ISSN 1091-6490. doi: 10.1073/pnas.1322611111.

[28] Quentin Chaboche, Gerardo Campos-Villalobos, Giuliana Giunta, Marjolein Dijkstra, Marco Cosentino Lagomarsino, and Vittore F. Scolari. A mean-field theory for predicting single polymer collapse induced by neutral crowders. *Soft Matter*, February 2024. ISSN 1744-6848. doi: 10.1039/D3SM01522J.

[29] Tyler N. Shendruk, Martin Bertrand, Hendrick W. de Haan, James L. Harden, and Gary W. Slater. Simulating the Entropic Collapse of Coarse-Grained Chromosomes. *Biophysical Journal*, 108(4):810–820, February 2015. ISSN 00063495. doi: 10.1016/j.bpj.2014.11.3487. URL http://arxiv.org/abs/1407.2850. arXiv:1407.2850 [cond-mat, physics:physics, q-bio].

[30] Hongsuk Kang, Philip A. Pincus, Changbong Hyeon, and D. Thirumalai. Effects of macromolecular crowding on the collapse of biopolymers. *Physical Review Letters*, 114(6):068303, February 2015. ISSN 0031-9007, 1079-7114. doi: 10.1103/PhysRevLett.114.068303. URL http://arxiv.org/abs/1409.5663. arXiv:1409.5663 [cond-mat, physics:physics, q-bio].

[31] Chanil Jeon, Youngkyun Jung, and Bae-Yeun Ha. Effects of molecular crowding and confinement on the spatial organization of a biopolymer. *Soft Matter*, 12(47):9436–9450, 2016. ISSN 1744-683X, 1744-6848. doi: 10.1039/C6SM01184E. URL http://xlink.rsc.org/?DOI=C6SM01184E.

[32] John F. Marko and Eric D. Siggia. Stretching DNA. *Macromolecules*, 28(26):8759–8770, December 1995. ISSN 0024-9297. doi: 10.1021/ma00130a008.

[33] Geoffrey Martin. On van't Hoff's Law of Osmotic Pressure. *Nature*, 70(1822):531–532, September 1904. ISSN 1476-4687. doi: 10.1038/070531b0.

[34] Theo Odijk. The statistics and dynamics of confined or entangled stiff polymers. *Macromolecules*, 16(8):1340–1344, August 1983. ISSN 0024-9297. doi: 10.1021/ma00242a015.

[35] Parth Rakesh Desai and John F. Marko. Molecular crowding suppresses mechanical stress-driven DNA strand separation. *Biophysical Journal*, 124(12):1886–1890, June 2025. ISSN 0006-3495, 1542-0086. doi: 10.1016/j.bpj.2025.04.024.

[36] P. G. de Gennes. *Scaling Concepts in Polymer Physics*. Cornell University Press, 1979.

[37] Zhiyu Cao and Peter G. Wolynes. Motorized chain models of the ideal chromosome. *Proceedings of the National Academy of Sciences of the United States of America*, 121(28):e2407077121, July 2024. ISSN 1091-6490. doi: 10.1073/pnas.2407077121.

[38] Norman F. Carnahan and Kenneth E. Starling. Equation of State for Nonattracting Rigid Spheres. *The Journal of Chemical Physics*, 51(2):635–636, July 1969. ISSN 0021-9606. doi: 10.1063/1.1672048.